



EUROPEAN
COMMISSION

Community Research



CARBOWASTE

*Treatment and Disposal of Irradiated Graphite and Other
Carbonaceous Waste*

Grant Agreement Number: **FP7-211333**



T-3.5.1

Topical Report with the characteristics of the legacy irradiated graphite

Author(s):

Gabriel Piña; CIEMAT (SP), Marina Rodríguez CIEMAT (SP), Eva Márquez (SP)

Document Number: CARBOWASTE-1307-T-3.5.1

Date of issue of this report: 01/06/2013

Start date of project: 01/04/2008

Duration: 60 Months

Project co-funded by the European Commission under the Seventh Framework Programme (2007 to 2011) of the European Atomic Energy Community (EURATOM) for nuclear research and training		
Dissemination Level		
PU	Public	
RE	Restricted to the partners of the CARBOWASTE project	
CO	Confidential, only for specific distribution list defined on this document	X

CARBOWASTE		
Work package: 3 Task: 3.5	CARBOWASTE document no: CARBOWASTE-1306-T-3.5.1 (e.g. May 2008 as date of issue: 0805)	Document type: T = Technical
Issued by: Ciemat (SP) Internal no.: CW1304-Technical Report 3.5.1		Document status: Final

Document title
<h2>Topical Report with the Characteristics of the Legacy Irradiated Graphite</h2>
Executive summary
<p>It is summarized the studies on Characterisation performed in 1990-1994 in the CEC project FI.2D.0017.ES (JR) and further characterisation program completed with the sampling of Vandellós 1 reflector. The legacy data are included in the CW-Data Base and confirm some of the conclusions and evidences founded in Carbowaste WP3 and WP4 project with more sophisticate techniques and in a deeper and wider way.</p> <p>Graphite manufacturing, from mineralogical and agglomerate components, has an important role in their characteristics. Graphite has a micro-crystalline structure together with more disorder areas irregular and with higher porosity. The graphite from Vandellós-1 and JEN-1 has a relatively high homogeneity structure being their crystalline structure highly graphitisation degree.</p> <p>It was measured the pore system according to IUPAC finding Macro and meso pores with variety of sizes and shapes. It was finding that the porosity increases when the graphite is treated. The poly-crystalline structure, with disorder areas, lead to a properties with a high influence in the irradiated graphite behaviour. The pore surfaces control the adsorption properties of graphite and some of their contents.</p> <p>The radioactive content depends on the storage in wet (reactor's pond) of the graphite, as happened with some fuel sleeves of Vandellós 1 graphite. The tritium content in this case is lower by nuclide interchange with water.</p> <p>The inventory finding (ordered in decreasing activity concentration) is: ^3H, ^{14}C, ^{60}Co and ^{134}Cs being tritium some orders of magnitude higher than the others. In general the origin is the activation of the impurities and the C of the structure in the case of ^{14}C, although in some of the analysed graphite comes from contamination coming from the fuel-cladding fissure in a neighbour fuel element. A complete characterisation</p> <p>Tritium speciation in graphite is in the majority of cases as HTO, Hydrocarbons or HT that can be volatiles or taking part or non or less graphitised areas, as recently Carbowaste work on speciation was conclude. Tritiated water is produced by mineral from environment than interchange tritium with surface layers of graphite. This water is release easily when the physical-chemical conditions are favourable. The accessibility of environment water to the pore system is fast at the beginning and very slow afterwards needed a long time of saturation. Nevertheless, the retained total amount of water is small.</p> <p>The rest of tritium is chemical bonded to graphite structure, probably in free positions in the microcrystal edges or in the more disorder areas formed part of hydrocarbon products with a certainly degree of freedom regarding to the graphite structure.</p>

The hydrocarbon compounds are stable at room temperature, but as the temperature is increasing the desorption of these is higher. Nevertheless, it is observed, at temperature higher than 400°C, carbon bonds breaking from less graphitised areas, together with desorption of hydrocarbons that drive to a generation of new hydrocarbon compounds.

Summarizing, the possibility of tritium release in gas form, as HTO from humidity interchange or -C-T in volatile hydrocarbon compounds as well, at environmental condition in quantitative amounts is practicably negligible. The radiocarbon is very stable, due to that in the majority of the case takes part of the structure being covalent bounded, even in the case that is in formed part of volatile hydrocarbon compounds it is needed temperatures higher than 250°C to be released. No other gaseous nuclides were studied in this project.

The nuclides release through liquid leaching is conditioned by the porosity of the graphite and the water-repellent characteristic of it. The water do easily not penetrate and the porosity leads to decrease the penetration ratio due to the surface tension.

The leachant chemical characteristics play an important role (specially the pH) to reach a leaching rate enough high, it is necessary acidic pH and/or presence of chloride ions. The kinetics of leaching was increased with the presence of complexants that produce the equilibrium between graphite surface and leachant displacement. The leaching rate of i-graphite in deionised water is small and no constant in tendency.

Revisions						
Rev.	Date	Short description	Author	Internal Review	Task Leader	WP Leader
00	dd/mm/yyyy	Issue	Name, Organisation <i>Signature</i>	Name, Organisation <i>Signature</i>	Name, Organisation <i>Signature</i>	Name, Organisation <i>Signature</i>
01	20/07/2013	First issue	G, Piña Ciemat	W. von Lensa FzJ	G, Piña Ciemat	G, Piña Ciemat
02	dd/mm/yyyy	2 nd Issue				

Table of Content

1	INTRODUCTION.....	7
1.1	Graphite Characteristics.....	7
1.2	Graphite of Moderator pile of Vandellós 1.....	8
1.3	Objectives.....	9
2	SAMPLES PREPARATION.....	10
2.1	Unirradiated Graphite.....	10
2.2	Irradiated Graphite	11
2.2.1	Graphite from the Sleeves of Vandellós 1	11
2.2.2	Graphite of Moderator Pile of Vandellós 1	11
3	STRUCTURAL CHARACTERISATION	14
3.1	X-ray Diffraction.....	14
3.2	Micro-morphology and absorption properties	17
3.2.1	N ₂ Adsorption	17
3.2.2	Hg Porosimetry.....	18
3.2.3	Density	21
3.2.4	Water absorption capability.....	21
3.2.5	Hydrogen Adsorption capability	24
3.2.6	SEM.....	25
3.2.7	Roughness Measurements	27
4	LOCATION OF IMPURITIES.....	29
4.1	Elemental Analyses.....	29
4.2	Hydrocarbon molecule contents.....	30
4.2.1	Thermal decomposition extraction	30
4.2.2	Solvent Extraction	35
4.3	Inventory determination of Sleeves of Vandellós 1	35
4.4	Inventory determination of Moderator of Vandellós 1	37
4.4.1	Determination of Tritium and Carbon-14.....	37
4.4.2	Determination of High Energy γ -EMITTERS.....	37
4.4.3	Determination of Pure β and β - γ Emitters	38
4.4.4	Determination of α -Emitters	39
4.4.5	Results	40
4.4.6	Discussion	47
5	CHARACTERISATION IN DECONTAMINATION STUDIES	49
5.1	Kinetics and Mechanism of hydrocarbon adsorption-desorption	49



5.1.1	Thermal treatment.....	50
5.1.2	Solvent Extraction	54
5.2	Kinetic and Adsorption mechanism of water	56
5.2.1	Results and Discussion.....	56
6	FINAL REMARKS.....	58
7	REFERENCES.....	60

1 INTRODUCTION

1.1 Graphite Characteristics

Graphite is a basically based carbon solid material that present a foil structure (Figure 1.1). In a layer each carbon atom is bonded to other three by sp² covalent bounds, being the bound distance small (0.142 nm). Different layers are parallel placed in the crystal bounded one to each other by weak Van der Walls interactions being the distance between two layers higher than covalent bounds (0.335 nm) [1]. The crystal has in average a wide around 250 nm and ≈ 100 nm in thickness. The solid is constituted by several crystal pile up in a more or less ordered way (Figure 1.2) [2] as is demonstrated in the work performed in the task 3.2. The inter-crystal spaces will be occupied with amorphous carbon which is 3D bounded with hetero-atoms as H, O, etc.

According to the packaging of C atoms in graphite, it is expected a density around 2.25 g·cm⁻³.

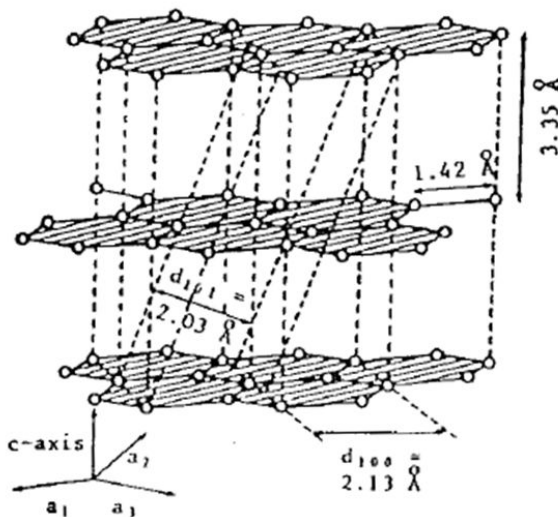


Figure 1.1 Graphite structure

However in the majority of the cases the density of a graphite block is lower than this figure due to the generation of a pore structure generate during the fabrication process.

Manufacturing process it is performed for example by Acheson process [3], in which is started with coke heating with silica in a furnace at 2500°C during 24-36 hours getting a powder product.

To get a determine form the powder is mixing with binder (synthetic resins, pitch or tar), obtaining a plasticene (modelling clay) that is highly accurate conformed. The graphite block obtained in this way is treated at 1000° C [4].

In this treatment a thermal decomposition of the binder in such a way that the more volatile materials are release from the structure given a by-product C enriched. This leads to the formation of pores and fractures in the block. The product obtained is graphitise at 2600-3000° C to graphitise the binder and a block of synthetic graphite is obtained [5]. The final product ia inner and surface porous graphite.

In this report characterisation performed on Vandellós 1 and Jen-1 virgin and irradiated graphite in the 90's is summarised. According to Waste Management Spanish National Plan and in the CEC project FI.2D.0017.ES

Data presented in this report comes from reflector, moderator and sleeves attending to the function in the reactor:



Figure 1.2 polycrystalline structure

- Graphite from Moderator: Only Vandellós 1 reactor has moderator pile and the mission is to moderate the fast neutrons from the fission to thermalize them in order to maintain the fission reaction of natural uranium [6]. There are two types of graphite pieces: the sleeves and the pile. The first are tubular pieces that cover the fuel elements. The pile pieces are hexagonal blocks with a central drill where the elements and sleeves are introduced.
- Graphite from Reflector: Both Jen-1 and Vandellos-1 reactor present reflector that constitute the periphery of the nucleus. In vandellos-1 the reflector is made with the same hexagonal blocks that the ones described in the moderator, but they haven't the central drill for the fuel element. The mission of reflector is to reflect into the nucleus the neutrons that escape from it and in this way improve the burning of the peripheral fuel elements.

The characterised graphite (Reflector and sleeves) has several disposal routes being necessary previous treatment and conditioning processes that are described in the original text but are out of the scope of this report.

1.2 Graphite of Moderator pile of Vandellós 1

Vandellós I Nuclear Power Plant consisted of a gas cooled type reactor moderated and reflected by graphite and cooled by carbon dioxide. It had a nominal throughput of 460 MWe and produced about 56000 GWh from its first coupled to the grid on 6th May 1972 to the last operation day on 19th October 1989, when a fire in conventional installations and without radiological consequences occurred.

The Spanish Government declared Vandellós I in definitive shutdown in July 1990 because of the high cost involved in recovering the plant to modern security standards. The responsibility of the plant was transferred from the original owner (Hifensa) to ENRESA for carrying out decommissioning activities after the unloading of the reactor, removing of nuclear fuel and conditioning and removing operating wastes.

Dismantling activities, until decommissioning Level 2, began in February 1998 and was scheduled for finishing at the end of 2002. As a consequence of those activities only the 20% of the site will remain as a regulated area including the reactor containment in a newly constructed outdoors-protective structure. A latency period of 25 years is scheduled for the starting of the final decommissioning activities until Level 3.

Quite important amounts of radioactive graphite arise in this type of nuclear reactors both during normal operation (tubular sleeves associated to each individual fuel element) and during dismantling (structural graphite pile acting as reflector and moderator and containing control rod and fuel channels).

Vandellós I moderator graphite pile is a vertical cylinder, 10.2 m height and 16.6 m diameter with a total weight of about 2680 tons. The total amount of graphite sleeves used during Vandellós I operation were about 181000 with a total weight of about 1000 tons.

From the waste management point of view, it is important to identify and quantify nuclides present in graphite waste. For this purpose, CIEMAT has developed a radiochemical characterisation project within the framework of CIEMAT-ENRESA co-operation agreement

where more than 200 powdered samples, taken during the conditioning activities of graphite sleeves, has been characterised and partial results were shown in a Spanish Nuclear Society Annual Meeting [7].

Previously to the end of the dismantling activities until Level 2, a drilling procedure was used for obtaining 58 cylindrical samples (50 mm height and 20 mm diameter) from graphite pile channels. Approximately all the samples were taken from channels located in the same semi-plane (between the central axis and the west part of the moderator graphite pile).

The aim of this paper is to present the determination procedures for characterising alpha, beta and gamma emitters in graphite samples and correlate the main results with the position in the graphite pile of the reactor.

Summarised results obtained from the radiological characterisation of these samples are given in this paper.

1.3 Objectives

The studies carried out in FI.2D.0017.ES dealt with several objectives:

- Determine the stability of the activation products
- Determine a method to remove nuclides from the graphite structure
- To seal the graphite against leaching

In this report only characterisation aspects are included and the studies are focused on:

- Determine the graphitisation grade and homogeneity of the graphite blocks.
- Determine the graphite impurities to understand the activation production mechanism
- Determine the pore volume and types [8,9,10,11]
- Determine the water absorption capability, in order to determine the leaching capability of graphite to release nuclides.
- Determine the Hydrogen content chemically bonded through radicals or hydrocarbon rests, in order to evaluate the possibility to find the chemical bounds of tritium in irradiated graphite.

It is known that irradiated graphite have different structural characteristics than virgin-graphite, due to the damage promoted by neutron flux in the reactor conditions, so that the second sets of objectives is

- To gasify with CO₂ to simulate through the corrosion the effects on the porosity that irradiation produces.

With irradiated graphite

- Characterise the Inventory of nuclides in irradiated graphite
- Localise the impurities in the structure

2 SAMPLES PREPARATION

2.1 Unirradiated Graphite

The unirradiated nuclear graphite to be studied are:

- A reflector JEN-1 element (GR.R.1) prismatic shape block, 760 mm length and 71x71 mm section with a weight of 7 kg
- A graphite sleeve from Vandellós-1 (GR.C.1) in cylindrical shape, 600 mm length, 135 mm external diameter, 123 mm internal diameter and 5.5 kg.

Both GR.R.1 and GR.C.1 called in the text R and C respectively, had been cut in order to get the following samples:

Powder Samples. Graphite block was milling in milling devices for getting to particle size ranges: 12-60 μm and 6⁺-100 μm

Massive Samples. R graphite was cutting in axial sections till obtained 71x16x16 mm prismatic pieces, on the other hand, C sample were cut in 4 circular slices with similar sizes.

The samples used to determine the homogeneity of original blocks are milling from specific points following the coordinates plotted in Figure 1. 3 samples of each graphite block: R1, R2, R3, C1, C2 and C3 were obtained

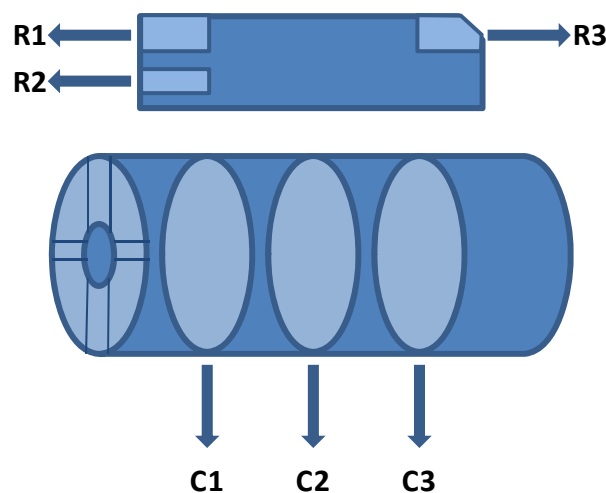


Figure 1.3 Getting Samples

Powder graphite samples R1 and C1 (60-100 μm) were gasified with CO_2 , by mean an horizontal furnace with a CO_2 (99.998%) flux of 80 ml/min. The heating ramp was 10° C/min till reach 925°C maintaining at this temperature 24 hours (samples RA1 and CA1) and 90 hours (samples RA2 and CA2). Burning % produced by gasification is determined by mass lost (weighting difference) obtaining the following values:

Table 2.1. Mass losses in gasification process

Reference	Gasification time (at 925° C)	Mass losses
RA1	24 hours	12 %
CA1	24 hours	14 %
RA2	90 hours	36 %
CA2	90 hours	47 %
RPA10	150 hours	10 %

Additionally a graphite R prism (71x16x16) was gasified with CO₂ in the same conditions as are described for powder samples varying the gasification time (Sample RPA10), obtaining a 10% of corrosion with 150 hours of treatment.

This loss of reactivity can be due to the sample size, massive samples has less surface to the oxidant gasses and the kinetic of the reaction is slower than in the case of powder samples.

2.2 Irradiated Graphite

2.2.1 Graphite from the Sleeves of Vandellós 1

Radioactive characterisation of i-graphite was performed on two types of sleeves from Vandellos-1 reactor; sleeves from the storage pond (wet sleeve) and sleeves storage out of the pond (dry sleeve).

The wet sleeve had suffered an isotopic interchange with the pond water that had contaminated via stored fuel elements. The dry sleeve is more or less representative (regarding the radioactivity content) of the moderator pile of plant.

The two wet sleeves (SI-1 and SI-2) were in the pond for 265 days and the burn-up was 45.07 and 62.65 Mw/day. The dry sleeve (SI-3) had a lower burn-up but it is unknown the actual value.

Sample preparation was carried out in the same way, making six cuts (figure 1.3) collecting the produced powder in each one separately [12]. In SI-1 powder from inner surface were collected and in SI-3 powder from both inner and outer surfaces were collected.

2.2.2 Graphite of Moderator Pile of Vandellós 1

Radioactive graphite presents special characteristics regarding to the radioactive waste characterisation process used in CIEMAT. Firstly the physical and chemical properties of graphite solid as well as powder that leads to develop special sample preparation processes and secondly the special radioactive content where majority components are ³H and ¹⁴C.

Cylindrical graphite samples were taken from the pile at several heights but in the same radial position, as it can be observed in Table 2.2, most of the time two samples were taken from neatly the same position (e.g. at 0.2 D and 9 m).

For extracting a powdered aliquot from the solid graphite cylinders a special method was adopted. The method consists on milling the cylinder in such conditions that dispersion of powder and consequent contamination are avoided.

Sample preparations required special techniques for homogenising the graphite powder in the ribbed planchets for gross alpha-beta determination; the graphite powder was spread on a filter paper, put on the planchet, using a cotton steak. In this way, the powder stands on the filter due to the static electricity. It is forming a homogeneous thin film that both adjusts to the calibration geometry and avoids self-absorption correction.

In order to get a stable and homogeneous counting geometry for direct gamma spectrometry a specific geometry based on a suspension of graphite powder in a gel, formed from Instagel® plus water, conditioned in a liquid-scintillation counting glass vial was used. This counting geometry assesses an adequate sample homogenisation along the sample counting time.

First characterisation step performed on all samples involves gross alpha and beta activity determination by proportional counter; 3H and 14C separated by catalytic combustion oven and determined by LSC. High-energy beta-gamma emitters such as: ²²Na, ²⁴Na, ⁵⁴Mn, ⁵⁸Co, ⁵⁹Fe, ⁶⁰Co, ⁶⁵Zn, ⁹⁴Nb, ⁹⁵Zr, ¹⁰⁶Ru, ^{108m}Ag, ^{110m}Ag, ¹²⁵Sb, ¹³⁴Cs, ¹³⁷Cs, ¹⁴⁴Ce, ¹⁵²Eu, ¹⁵⁴Eu, ¹⁵⁵Eu and ²⁴¹Am were directly measured.

Second characterisation step was performed on some selected samples (G-5, G-13, G 16, G-23, G-30 and G-37). These samples were solubilised in acidic media and radiochemical processes for pure beta emitters: ³⁶Cl, ^{41/45}Ca, ⁶³Ni, ^{89/90}Sr and ²⁴¹Pu beta-gamma emitters: ⁵⁵Fe, ⁵⁹Fe, ⁵⁹Ni, ^{93m}Nb and ⁹⁴Nb and the most significant alpha-emitting radionuclides: ²³⁸Pu, ^{239/40}Pu, ²⁴¹Am, ²⁴²Cm, ²⁴⁴Cm and ^{234/238}U were performed.

Positions of the reference samples are shown in Table 2.2.

Table 2.2 Positions and references of the samples extracted from de graphite pile

Height (m)	Approximate distance from the graphite pile axis (D = moderator graphite pile diameter)										
	0.0 D		0.1 D		0.2 D		0.3 D		0.4 D		0.5 D
9.0	G-3	G-6	G-14	G-22	G-30	G-38	G-41	G-44	G-47	G-58	G-50
7.7			G-13	G-21	G-29	G-37			G-57		
6.3			G-12	G-20	G-28	G-36			G-56		
5.1			G-11	G-19	G-27	G-35			G-55		
3.9	G-2	G-5	G-10	G-18	G-26	G-34	G-40	G-43	G-46	G-54	G-49

3.3			G-9	G-17	G-25	G-33			G-53		
1.5	G-1	G-4	G-8	G-16	G-24	G-32	G-39	G-42	G-45	G-52	G-48
0.4			G-7	G-15	G-23	G-31			G-51		

3 STRUCTURAL CHARACTERISATION

3.1 X-ray Diffraction

The XRD data were obtained using a diffractometer SEIFER JSO DEBYE FLEX 2002 OVER un-irradiated powder samples (12-60 μm) of both original and gasified.

To check the micro-structural homogeneity of virgin R (from reflector) and C (from Sleeve) graphite X-Ray Diffractograms were obtained from powder samples R1, R2, R3 and C1, C2 and C3, and are compiled in table 3.1:

Table 3.1 XRD data for graphite R and C

Sample	2 θ	D (Å)	I _{rel}	I _{max}	Sample	2 θ	D (Å)	I _{rel}	I _{max}
R1	23.8	3.74		70	C1		3.74		177
	26.4	3.37		1041			3.38		9628
	27.2	3.27	0.7	6		23.8	3.28	1.8	300
	42.5	2.13	100.0	160		26.4	2.13	100.0	118
	44.3	2.04	1.5	107		27.2	2.05	3.1	156
	54.4	1.68	1.0	171		42.5	1.69	1.2	393
	77.4.	1.23	1.6	442		44.3	1.23	1.6	115
			4.2	105		54.4		4.1	
			1.0			77.4.		1.2	
R2	23.9	3.73			C2		3.74		112
	26.5	3.36		111			3.38		8823
	27.3	3.26	1.0	1131		23.8	3.28	1.3	195
	42.5	2.13	100.0	4		26.4	2.13	100.0	92
	44.4	2.04	1.6	178		27.2	2.05	2.2	125
	54.5	1.68	0.8	85		42.4	1.69	1.0	376
	77.5.	1.23	1.3	150		44.4	1.23	1.4	83
			4.0	452		54.3		4.3	
			0.9	102		77.4.		0.9	
R3	23.8	3.74			C3		3.74		122
	26.4	3.37					3.37		9612
	27.2	3.27	1.2	122		23.8	3.27	1.3	212
	42.4	2.13	100.0	1033		26.4	2.13	100.0	79
	44.3	2.04	1.9	2		27.2	2.05	2.2	110
	54.4	1.69	1.1	195		42.5	1.69	0.8	408

			1.8			44.2		1.1	
	77.4.	1.23		114			1.23		72
			4.1	189		54.4		4.2	
			1.0	428		77.5.		0.8	
				10					

The first remark on the results in Table 3.1 is that the diffraction angles are the characteristic ones of graphite, that means that with the XRD technique we cannot appreciate another compounds in the samples analysed.

The higher intensive peak that corresponds to the interlayer distance can be observed at $2\theta = 26.4$ for both (R and C) graphite samples.

Comparing the Values of maximum intensity (I_{max}) of this peak for R1, R2 and R3 or among C1, C2 and C3, it is observed that $R2 > R1 \approx R3$ and $C2 > C1 \approx C3$, being the differences homogeneous, although the graphitisation degree in the bar (R) is higher in the inner part that in the surface and in the sleeve (C) slightly higher in the centre than in the extremes.

The I_{max} for R is higher, in the range 7-20%, regarding C that indicates a higher graphitisation degree in R and consequently the less reactivity in gasification process regarding C. The time and temperature of reaction was the same for R and C (925° C for 24 h and 90 h) obtaining corrosions % of 12% (RA1) and 36 % (RA2) and 14% (CA1) and 47% (CA2).

Table 3.2 collect the data of XRD for the powder CO₂ gasified graphite (RA1, RA2, CA1 and CA2) and in order to compare with no gasified graphite the values of R1 and C2.

Table 3.2 XRD data for gasified R and C graphite

Sample	2θ	D (Å)	I _{rel}	I _{max}	Sample	2θ	D (Å)	I _{rel}	I _{max}
R1	23.8	3.74		70	C2		3.74		112
	26.4	3.37		1041			3.38		8823
	27.2	3.27	0.7	6		23.8	3.28	1.3	195
	42.5	2.13	100.0	160		26.4	2.13	100.0	92
	44.3	2.04	1.5	107		27.2	2.05	2.2	125
	54.4	1.68	1.0	171		42.4	1.69	1.0	376
	77.4	1.23	1.6	442		44.4	1.23	1.4	83
			4.2	105		54.3		4.3	
			1.0			77.4		0.9	
RA1	23.8	3.73			CA1		3.74		150
	26.4	3.37					3.37		8695
	27.3	3.27	1.7	144		23.8	3.26	1.7	227
	42.4	2.13	100.0	9832		26.4	2.13	100.0	126
	44.5	2.04	2.1	209		27.2	2.04	2.6	212

			1.0			42.4		1.4	
	54.5	1.68		76			1.68		366
	77.4	1.23	2.0	213		44.3		2.4	141
			4.4	426		54.4		4.2	
			1.6	133		77.4		1.6	
RA2	23.8	3.73			CA2		3.73		122
	26.4	3.37					3.37		9612
	27.3	3.26	1.5	144		23.8		1.4	212
	42.4	2.13	100.0	9832		26.5		100.0	79
	44.4	2.04	2.1	209		27.3		2.6	110
	54.5	1.68	0.8	76		42.4		1.3	408
	77.4	1.23	2.2	213		44.3		2.3	72
			4.3	426		54.5		4.5	
			1.4	133		77.4		1.3	
RPA10	23.8	3.73							
	26.5	3.36							
	27.3	3.26	1.0	111					
	42.5	2.13	100.0	1075					
	44.4	2.04	1.3	144					
	54.5	1.68	0.7	74					
	77.5	1.23	1.4	151					
			4.1	445					
			0.9	99					

Gasified material maintains crystallinity parameters and maximum intensity peak positions, that indicates that gasification does not imply an structural change.

Similar results are obtained for the gasified block sample (RPA109 who was milled before XRD measurement).

3.2 Micro-morphology and absorption properties

3.2.1 N₂ Adsorption

N₂ adsorption isotherms at 77 K were measurement for R1, R2, R3, RA1, RA2 and C1, C2, C3, CA1, CA2 had been carried out on powder samples (60-100 μm) in a COULTER OMNISORP 100CX are plotted in Figures 3.1 and 3.2.

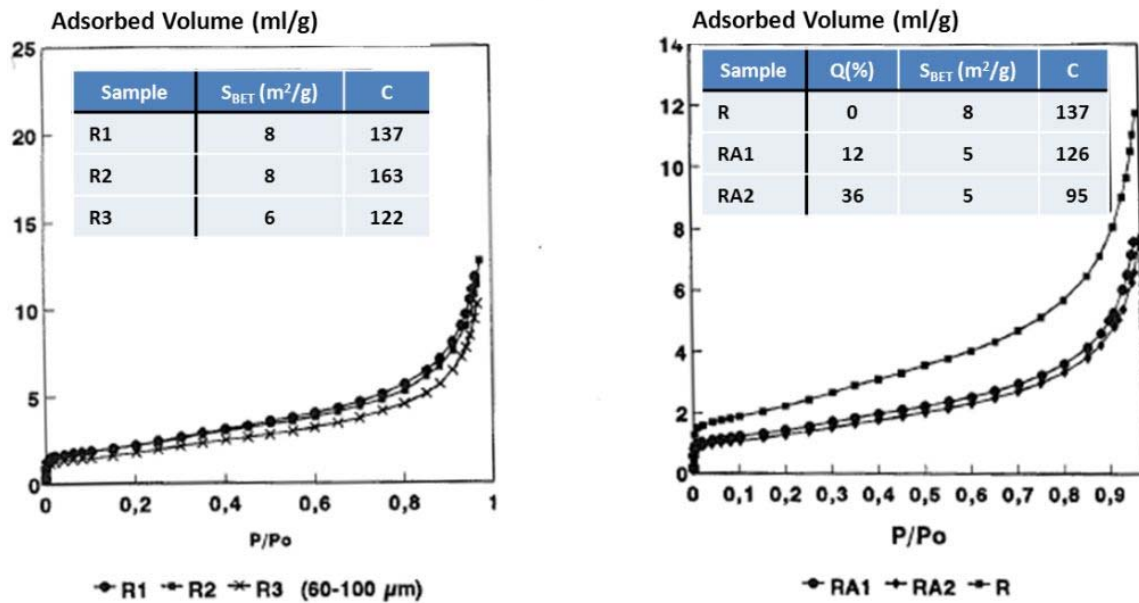


Figure 3.1 N₂ Adsorption Isotherms at 77K of JEN-1 Reflector Graphite
Virgin graphite (on the left) and gasified graphite (on the right)

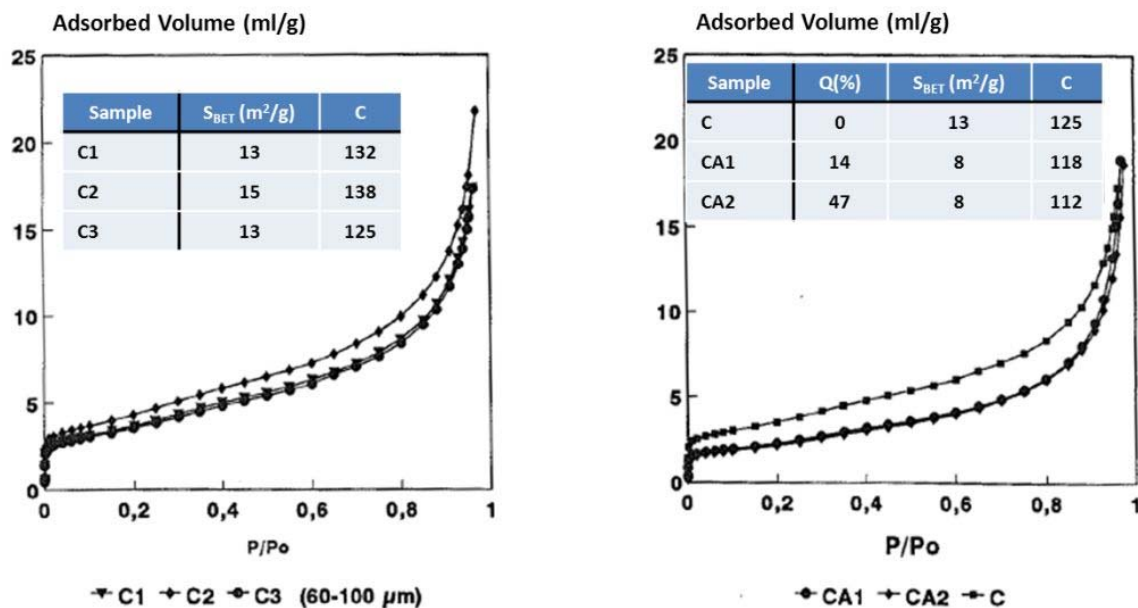


Figure 3.2 N₂ Adsorption Isotherms at 77K of Vandellós-1 Sleeve Graphite
Virgin graphite (on the left) and gasified graphite (on the right)

Bet analyses give the specific surface and C parameter that gives the information about the interactions in the surface with the adsorbed gas (N_2). The values are plotted inside the aforementioned figures where is observed:

- Adsorption isotherms, in every case, are characteristics from a non-porous solid, due to the found adsorbed amounts are low, increasing to $P/P_0 > 0.3$ as a consequence of multilayer adsorption.
- The homogeneity degree of the original bar is in the normal range. Small differences are appreciate in the sleeve (C2 regarding C1 and C3)
- The surface of the sleeve graphite (C) is around double than the one of graphite from the reflector (R) in the order of 13-15 m^2/g vs. 6-8 m^2/g . This effect is another evidence of the higher graphitization degree of R vs. C obtained in XRD studies.

Observed the results of N_2 adsorption isotherm at 77K of RA1, RA2 or CA1, CA2 gasified graphite it is deduced that:

- The surface is reduced for both C and R gasified graphite in a similar factor.
- The C parameter in BET equation decrease as the gasification increase and the phenomenon is higher for reflector graphite (R).

The tendency of both parameters indicates that gasification increase the surface homogeneity. Possibly the most disorder carbon together with the smaller crystals were eliminated during gasification remaining the most homogeneous and ordered graphite with smaller specific surface and consequently with lower interaction with N_2 .

3.2.2 Hg Porosimetry

The pore size of macropores and mesopores (7500-75 nm) was obtained using a Carlo Erba series 200 Porosimeter.

Two type of samples were measured: powder graphite (\varnothing : 60-100 μm) for samples R, RA1, RA2 and C, CA1, CA2 and grain samples (\varnothing : 1-3 mm) from only one sample of R and C graphite.

The refilling of the dilatometer with Hg at 10^3 torr (in order to avoid air inclusion), the graphite samples were dried at 120°C for 16 hours.

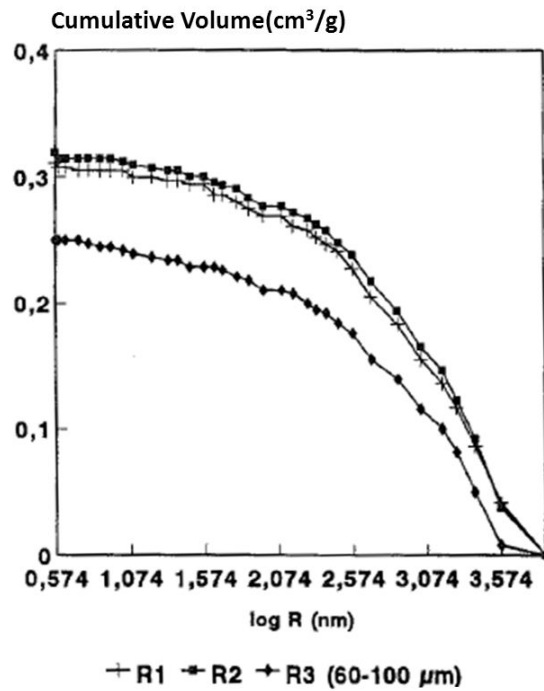


Figure 3.3 Hg porosimetry of JEN-1 reflector

In Figure 3.3 it is represented the cumulative volumes distribution of macropores and mesopores (range 7.5-7500 nm) for the different non-gasified samples in powder (60-100 μm), from the reflector (R1, R2 and R3) and from the sleeve (C1, C2 and C3).

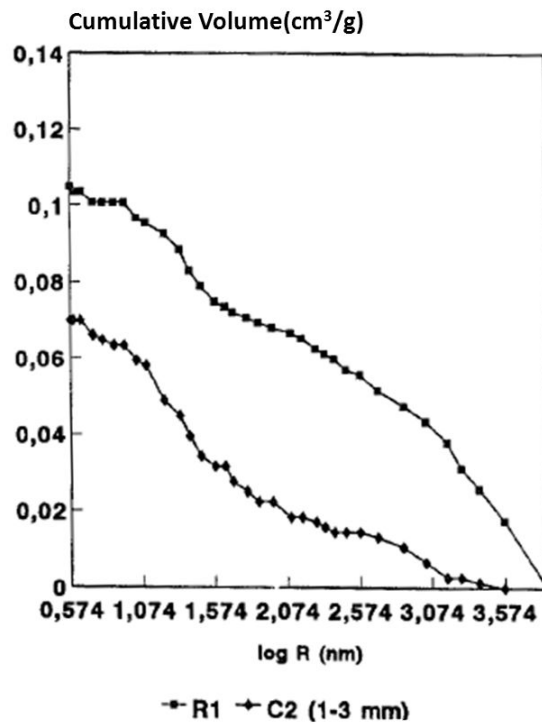


Figure 3.4 Hg porosimetry

In Figure 3.4 this is observed the higher pore volume is found at radii < 300 nm for R graphite and radii < 200 nm for graphite C. That means the majority of the porosity is concentrate in the high radius macropore range.

The volume registered it is not the same for the same type of graphite. The curves of R1 and R2 are similar but different to the one of R3. These differences can be caused by the experimental system due to it cannot distinguish between pores and inter-particle volume whose is expected to be non-negligible taking into account the particle size in these graphite types.

According to the pore classifications by IUPAC [13] the border line between macropores and mesopores is marked at 50 nm ($r = 25$ nm), from the aforementioned curves the volume of mesopores ($25 < r < 7.5$ nm), not included the macropores due to the possibility to be overestimate by the inter-particle spaces (Table 3.3).

It is remarkable that the graphite investigated graphite have a small mesopore volume but non-negligible, and these mesopore volume in higher in sleeve graphite (C) than in reflector graphite (R) which confirms the BET results.

The results when the particle size is in the range 1-3 mm) the curves shape change (Figure 3.5) in both ranges macropores and mesopores and the total deduced volume is lower for grain samples (1-3 mm) than for powder samples (12-60 μ m), this experiences were performed in two replicates obtaining reproducible results. It looks that a part of the porosity of the graphite grains were not available to the Hg, this effect it was not present when the graphite grains were milling into powder. However, comparing the quantification of mesopore volume in the powder samples with the ones of the grain samples it was observed that the mesopore volume of grain samples is 40% higher than in powder samples (0.014 vs 0.021 cm^3/g for R samples and 0.018 vs 0.030 cm^3/g for C (sleeve) samples), that indicates a possible destruction of mesoporosity in the milling process.

Table 3.3 Pore volume determined by Hg Porosimetry

Sample	Mesopore Volume ($r < 25$ nm) (cm^3/g)		Macropore Volume ($r > 25$ nm) (cm^3/g)
	Powder (60-100 μ m)	Grain (1-3 mm)	Grain (1-3 mm)
R1	0.014	0.021	0.079
RA1	0.003		
RA2	0.000		
C1	0.018	0.030	0.040
CA1	0.016		
CA2	0.016		
RPA-10	0.009		

From the values of Table 3.3 we can induce that the mesopore volume for Reflector graphite is lower than for Sleeve graphite in powder and grain samples. In grain samples it was possible to study the macroporosity and it is observed that in reflector graphite the macropore volume is higher than in the sleeve graphite (0.083 vs. 0.040 cm^3/g).

On the other hand the Hg porosimetry of the gasified samples showed that the mesopores, volume decrease as the time of gasification decrease for both series (R and C), specially in

the first activation phase. The most relevant differences were found when series R and C were compared. The gasification of R graphite drove to a sample without mesopores ($R > 7.5$ nm) meanwhile in C graphite maintain the value $0.016 \text{ cm}^3/\text{g}$.

A part of the prismatic block RPA-10 was milling to $60\text{-}100 \text{ }\mu\text{m}$. Mesoporosity values (Table 3.3 orange column) were, as was expected, in the range between gasified and non gasified material due to the mix of graphite in this case.

3.2.3 Density

Density measurements were performed on three prismatic samples of reflector graphite (R) with different sizes ($71 \times 17 \times 17$, $34 \times 17 \times 2$ and $8 \times 4 \times 2$ mm) by water and mercury picnometry.

For density determination with Hg picnometry the refill was performed at low pressure (10^{-2} torr), in order to avoid the air inclusion in the mercury that introduce uncertainty in the measurement.

It is obtained that density values by water picnometry depends on the contact time between sample and water, which indicates the high porosity volume in the graphite samples. In every experiment the contact time was 24 hours.

Density values of graphite R are in table 3.4

Table 3.4 Density determinations

Size (mm)	ρ_{Hg} (g/cm^3)	$\rho_{\text{H}_2\text{O}}$ (g/cm^3)	Volume access to water (cm^3/g)
71x17x17	1.72	1.78	0.019
34x17x2	1.74	1.94	0.032
8x4x2	1.82	1.97	0.042

It is observed that density measurement by Hg or water (contact time 24 h.) slightly increase as the sample size decrease, being in every case lower than the one expected for pure graphite ($2.25 \text{ g}/\text{cm}^3$). Considering high purity and crystallinity in the studied graphite the difference of density can attribute to the sample porosity, the pore system is more available to liquid occupation as the sample block is smaller.

The pore volume accessible was calculated from the density values (Table 3.4). This volume is not negligible taking into account that the pore sizes higher than $7.5 \text{ }\mu\text{m}$ are occupied by Hg in the density assay and are not considered in the calculation. This pore fraction ($>7.5 \text{ }\mu\text{m}$) can be calculate from the density difference from Hg picnometry ($\approx 1.75 \text{ g}/\text{cm}^3$) and the normal graphite density ($\approx 2.25 \text{ g}/\text{cm}^3$) that indicates a $0.13 \text{ cm}^3/\text{g}$. This indirect calculated value is only a tendency but there are not doubts about the presence of pores $>7.5 \text{ }\mu\text{m}$ in the nuclear graphite treated.

The pore volume accessible to water and non accessible to Hg, increase as the sample size decrease that indicates that the kinetic to difusse the water inside the pore system was slow.

3.2.4 Water absorption capability

The water adsorption was performed on graphite blocks and powder samples by four procedures [14]:

- a) By immersion of graphite blocks from C, R and RPA-10 (17x17x17 mm) in water at room temperature: The block is suspended from the weighting device by a nylon wire and immerse into water, registering the weight. Several weighting measurements were done at time intervals keeping the level of water and sample continuously suspended from the weighting device. The increase of weight was considered the adsorbed water amount.
- b) Introducing powder graphite R (60-100 μm) into a 100°C steam atmosphere. The system set-up consists on an autoclave half filling with water and introducing the samples on a holder device, in such a way that graphite never touch the liquid water. Heating the device at 100° C the steam generated is adsorbed by the graphite. The increase of weight is registered at different process times regarding the original weight is the water adsorption capability
- c) Water adsorption by introducing the sample in a thermostatic close camera humidity saturated. Here two set of experiment were performed:
 - a. To determine the adsorption capability in function of particle size and block sample sizes. Powder graphite R (60-100 μm) and prismatic blocks: 71x17x17, 34x17x2 and 8x4x2 mm. The samples introduced in the camera were weighted at time intervals and stopped at 120 hours where adsorption equilibrium is reached. This experiment tries to indicate the amount of water adsorbed by a graphite brick (real size).
 - b. To compare the water adsorption-desorption capability of Reflector (R) graphite and sleeve (C) graphite whose were cutting in prismatic pieces 3.7x4.2x1.9 mm size and were measured in a saturated humidity sealed camera at 25°C and 30°C (water partial pressure 23.76 and 31.82 mm Hg). The weight is register till stabilization, that means reach the apparent equilibrium (approximately 100 h)
- d) By controlled thermal desorption and volatile analyses by IR spectrometry. These assays are described afterwards due to the objective are different than the one in this section.

The assays corresponding to c)b. Are the ones presented due to the more reliable results according to the real conditions.

To estimate the water amount that a graphite block could retain from the environment, different particle sizes graphite blocks.

The water adsorption kinetics at 25°C ($P_{H_2O} = 23.76$ torr), for graphite R is in figure 3.6 for different particle size blocks and powder. In this figure is observed that the curves obtained in every case are in the same shape, it means that the water amount is quickly adsorbed and is stabilized around 100 hours contact time. The most remarkable differences are found when the particle size changes. From powder to blocks, even if the block is small (3.7x4.2x1.9 mm), the decrease observed is dramatic: from 3.5% to 0.5%, showing lower differences when the block size increase.

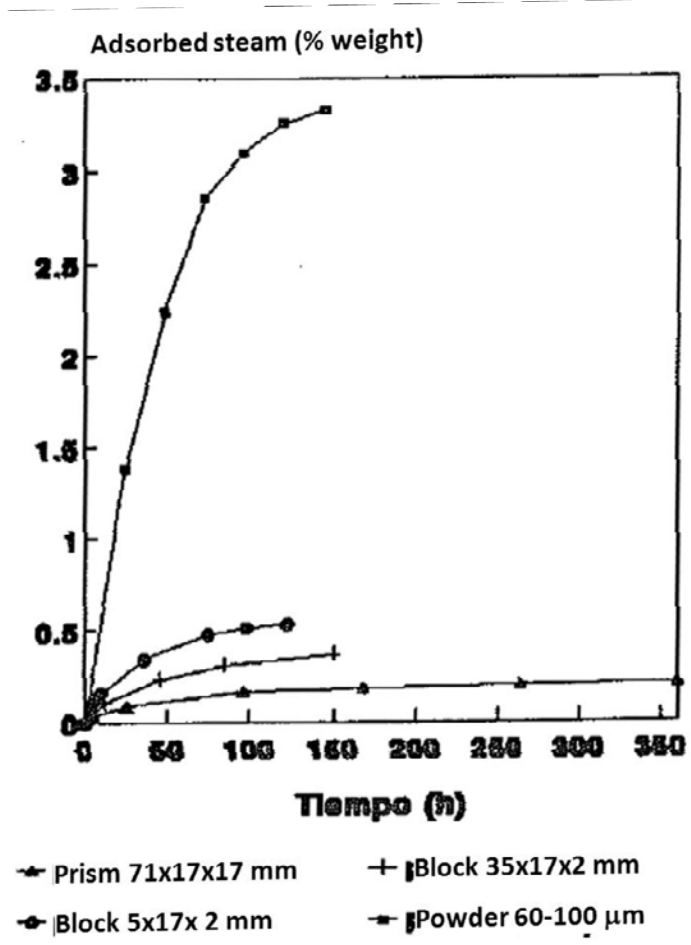


Figure 3.5 Water adsorption in function of particle size

These differences can be due to a porosity non accessible to water (close porosity o contracted pores that block or avoid the fluency of water, increasing in this way the adsorption surface.

To correlate the adsorbed water amount in function o block sizes, it was considered the ratio between geometric surface and volume of samples (S_g/V) and represented versus the retained water amount at 50 hours and 100 hours (Figure 3.6) It is remarkable the decrease of adsorption capability as the block size increase that follows and exponential trend. In this way, the estimation of water retention, of graphite brick (reactor size), is in the order of 0.1%.

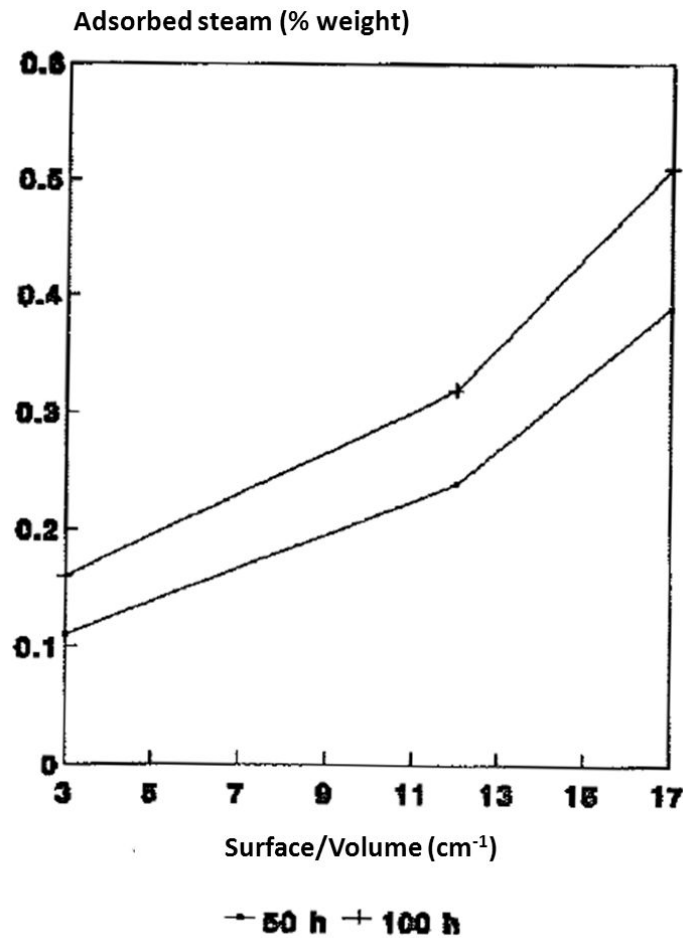


Figure 3.6 Water adsorption in function of sample size

3.2.5 Hydrogen Adsorption capability

3.2.5.1 Experimental

Graphite blocks for reflector (R) and sleeves (C) (71x17x17 mm) were put into a horizontal glass pipe at 20°C. H₂ current is passing through for 6 h. at 120 ml/min. Control weight is performed after adsorption process. The experiment was repeated at 300° C, introducing the sample in the furnace and heating in a slope of 5° C/min till reach the target temperature. The H₂ current is maintained during whole process.

3.2.5.2 Results and Discussion

There are not weight variation for graphite R and C putting in H₂ current at room temperature, that means R and C graphite not adsorbs H₂ at room temperature. This behaviour is the one predictable for graphite that is in contact with air for long period, as is the case assayed. The atoms placed in the vertex of the crystals are the ones capable to chemisorb hydrogen and normally are saturated during the manufacturing process, chemisorbing organic radicals from the cracking of pitch in the graphitization process or chemisorbing oxygen from the air it is described in the literature that nuclear graphite adsorbs oxygen from the air even at -30° C).

So that at room temperature the only one process to adsorb H_2 is the physisorption and the expected retained H_2 amounts are negligible.

If the graphite is treated at higher temperature ($300^\circ C$), a mass loss is registered possibly due to a reduction of the oxygen chemisorbed in the surface of the graphite with the consequent evolution to H_2O .

3.2.6 SEM

3.2.6.1 Experimental

Graphite prismatic specimens from reflector (R) and gasified with CO_2 (RPA-10) $3.7 \times 4.2 \times 1.9$ mm size had been studied using a Scanning Electron Microscope JEOL mod JSM-840 (Figure 3.7) in order to compare the surface changes after and before gasification. Additionally the deep of the CO_2 reaction in the graphite surface was checked.



Figure 3.7 Scanning Electron Microscope: JEOL mod JSM-840

3.2.6.2 Results and discussion

A direct observation of the polished graphite R specimens showed the presence of numerous pores in a wide range of size and shape. This pores comes from the graphite manufacturing as a consequence of the differential contraction of agglomerate material (pitch) in the graphitisation process at high temperature, realising, in a part, volatile material at the same time.

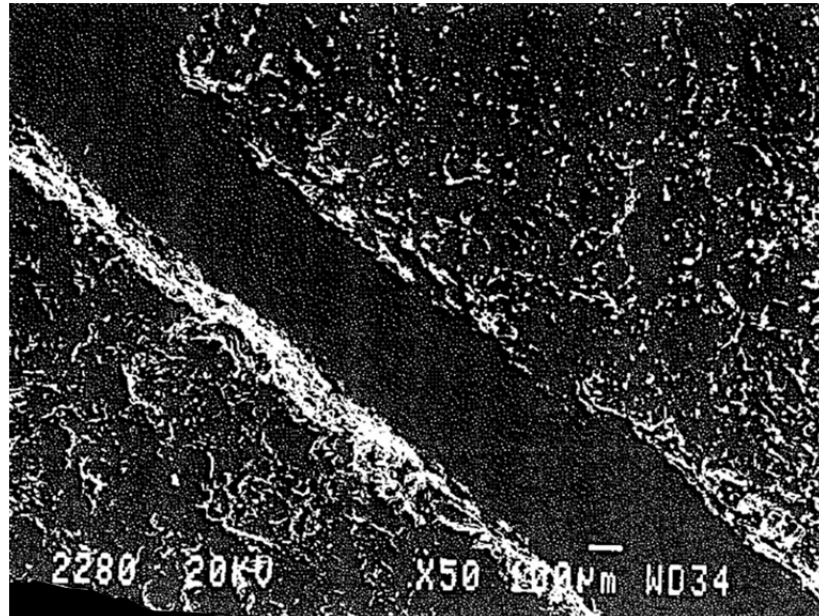
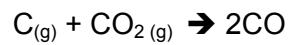


Figure 3.8 Gasification effect observed by SEM

Figure 3.8 compares the surface of the prismatic specimen of graphite R and gasified graphite R (RPA-10). The presence of more and larger pores in the surface of RPA-10 is the consequence of gasification:



The attack was produced on specific zones, that are the most reactive areas that could correspond with the vertex of microcrystals of graphite.

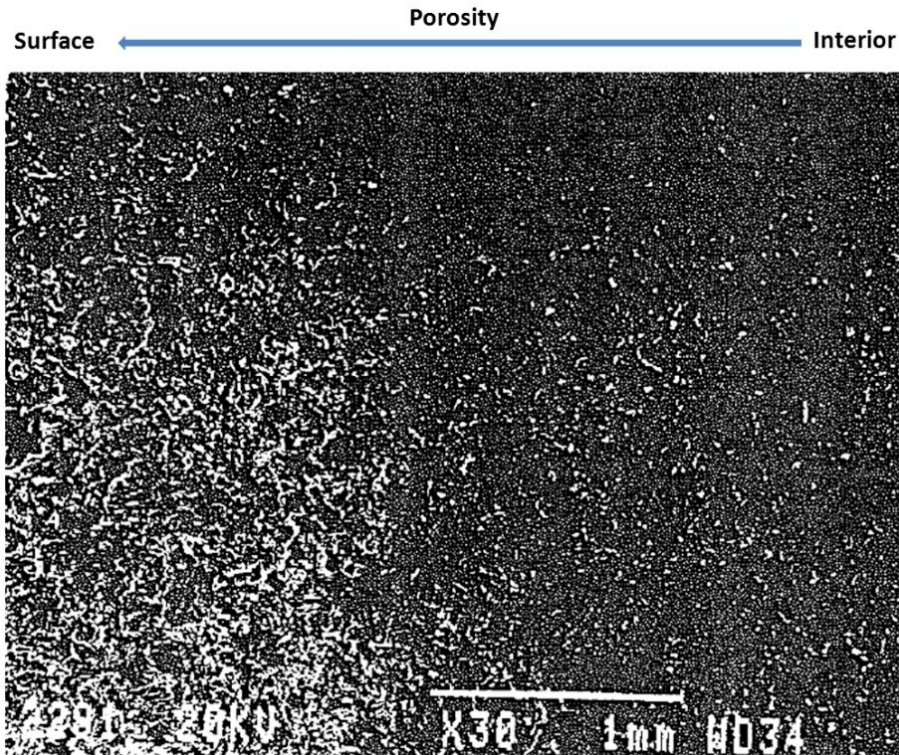


Figure 3.9 In depth gasification effect

When the porosity of gasified graphite is observed, regarding the distance to the surface, the gasification is not homogeneous. In figure 3.9 we can observe a major pore size in the surface than in the inner parts due to CO_2 gasification. Going into the specimen the pore size decrease in such a way that at 1.5-2 mm depth the porosity is the same that the one of R graphite. This behaviour is attributed to the CO formation during the reaction, that inhibit the reaction and avoid the penetration of CO_2 in the material.

3.2.7 Roughness Measurements

The Roughness measurement technique allows to determine the topography in a determine direction of the test specimen by mean the recorder from a surface-marker ($\varnothing=25 \mu\text{m}$) along the way of the surface selected. The apparatus used was a SF200 Planner Industrial that allows selecting vertical range between 2 and 100 μm .

Data Analyses from the recorded data of the roughness measurement (peak area, average values, etc.) two are selected:

- R_{max} , that is the higher difference value between the peak and the minimum found in the studied surface and
- $R_{Z_{DIN}}$ that is the arithmetic average of all differences between the maximum and the minimum in specific surface intervals l_e . In the case of the one represented in Figure 3.10:

$$R_{Z_{DIN}} = \frac{1}{5}(z_1 + z_2 + z_3 + z_4 + z_5)$$

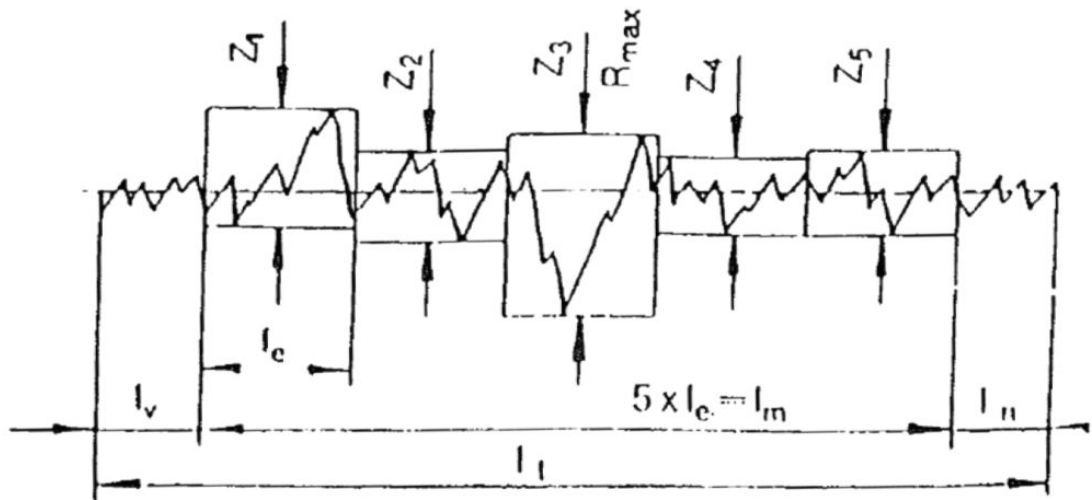


Figure 3.10 Graphite R roughness analysis

3.2.7.1 Results and Discussion

The profiles of the specimens determined by this technique (Figure 3.11), show the presence of deep surface irregularities. The origin of these is difficult to determine due to that is not possible to distinguish between small pores or defects in the polish process. In any case in the high deep pores is determined depth $>8 \mu\text{m}$.

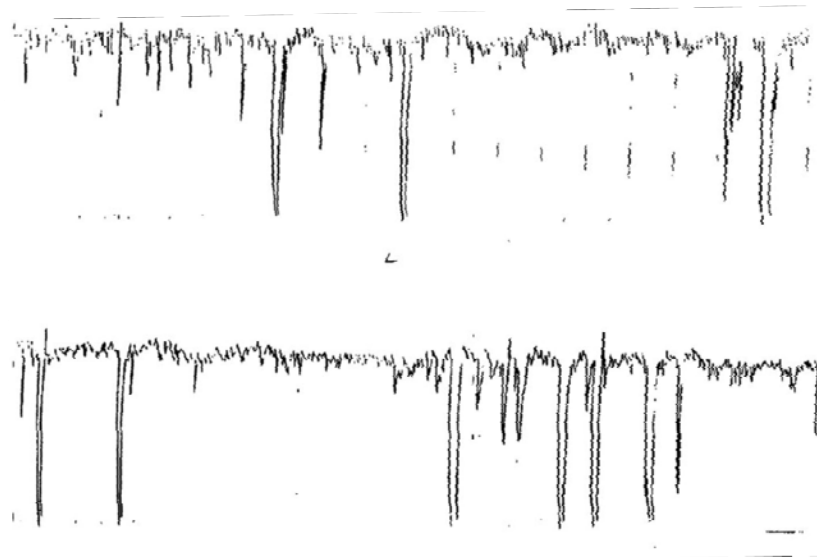


Figure 3.11 Roughness analysis

4 LOCATION OF IMPURITIES

4.1 Elemental Analyses

Elemental analyses was carried out using Atomic absorption analyses (Table 4.1) on powder samples coming from the powder generated in the cutting of a virgin sleeve (14) following the Figure 4.1.

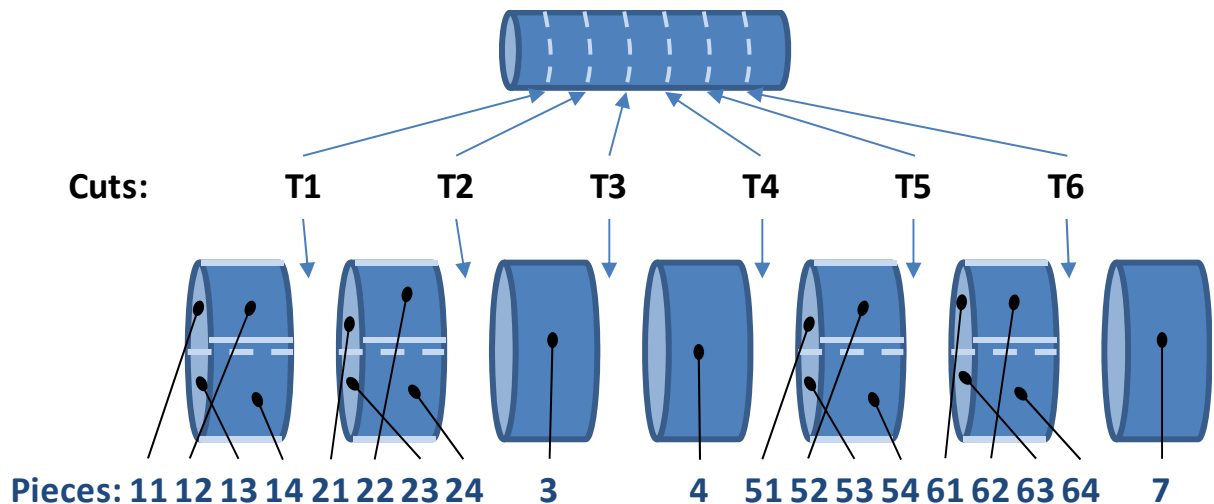


Figure 4.1 Sleeve cuts and pieces

Table 4.1 Elemental analyses of Vandellós 1 Virgin graphite by Atomic Absorption

Element	Concentration (ppm)					
	T1	T2	T3	T4	T5	T6
Al	1,7	1.6	2.0	4.6	6.8	1.0
As	<1					
B	0.1					
Ba	0.64					
Be	<0.15	<0.15	<0.15	<0.15	<0.15	<0.15
Bi	<1.0					
Ca	8.5	<12	<12	<12	<12	<12
Cd	0.83	<0.3	<0.3	<0.3	<0.3	<0.3
Co	<0.25	<0.25	<0.25	<0.25	<0.25	<0.25
Cr	0.42	<0.6	<0.6	<0.6	<0.6	<0.6
Cs	<0.20					
Cu	3.7					
Fe	36	7	5.8	4.9	7.1	4.0
Li	<0.05	<0.05	<0.05	0.08	0.08	<0.05
Mg	<2.0					
Mn	0.24	0.24	0.24	0.24	0.24	0.24
Mo	0.54	<0.3	<0.3	<0.3	<0.3	<0.3
Na	10	13	<12	<12	<12	<12
Ni	5.6	11	4.4	4.9	13	4.9
Pb	<0.25	3.9	2.8	2.4	1.2	0.78
Se	<1.0	<2.5	<2.5	<2.5	<2.5	<2.5

Sr	<0.15	<0.15	<0.15	<0.15	<0.15	<0.15
Tl	0.34					
V	9.5	11	8.5	2.6	3.8	14
Zn	1.7					

4.2 Hydrocarbon molecule contents

Hydrogen in graphite can be found in three forms as water, as gaseous H₂ or as heteroatom bounded to the graphite structure, possibly as a part of hydrocarbon. To determine the content and the location of this three forms two procedures were used: Thermal decomposition and solvent extraction.

4.2.1 Thermal decomposition extraction

In general terms this procedure is based on heating in a determine sequence the graphite in inert or oxidizing atmospheres in order to break or decompose the lighter structures in it. The decomposition products can be detected by different techniques.

When atmosphere is oxidizing the Carbon react to CO₂ and CO and hydrogen is oxidized to H₂O, breaking some chemical structures by oxidation effect. When the atmosphere is inert the free molecules at treatment temperature are released without transformation or reacting with the molecules chemisorbed in the surface. In oxidizing atmosphere from 450° C starts the combustion and the graphite is corroded.

The thermal decomposition and the analysis of the reaction products were carried out by different methods

4.2.1.1 Thermo gravimetry and DSC

Twenty grams of powder graphite R (60-100 μm) was used for thermal treatment in the holder of a CI Instruments thermo-balance. In N₂ atmosphere (60 ml/min) the graphite was heating at 20° C till 900 ° C and maintaining during 1 hour. The gasses were measured connecting the thermo-balance to a Gas Chromatograph –MS VG quadrupole.

In the detection of volatile materials by thermo-balance connecting to a GC-MS for a ≈0.35 g of graphite, the mass lost detected during the heating process was ≈7E-4 g. This mass from volatile materials during 20 minutes of experiment duration gives a weak signal which was not possible to evaluate.

However it was possible to determine in function of the desorption temperature in the thermo-balance (figure 4.2)

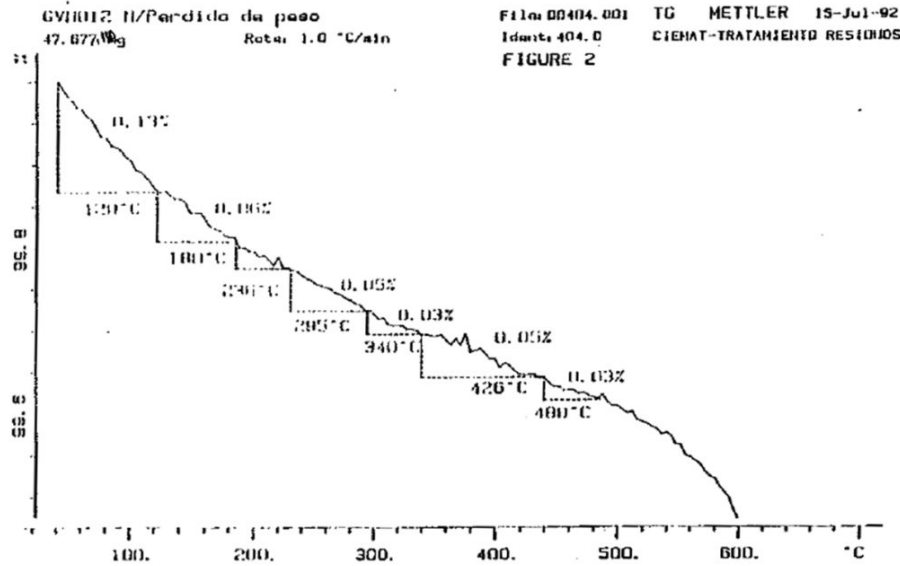


Figure 4.2 Graphite Thermo-gravimetry

Similar results were obtained by Differential Scan Calorimetry (DSC)

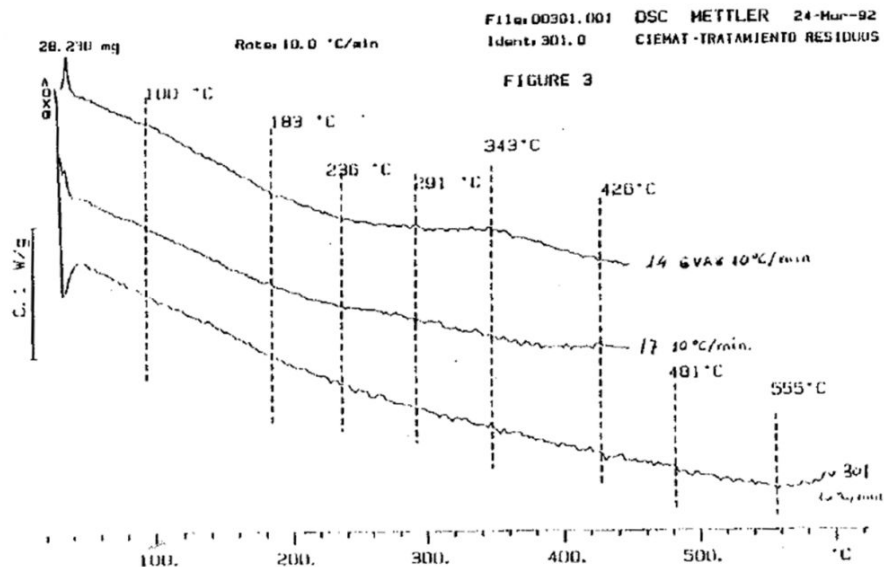


Figure 4.3 Graphite Thermo-desorption Scanner

4.2.1.2 Mass Lost by heating

The thermal treatment was performed heating in N₂ atmosphere, 35 g of graphite R and 35 g of graphite C in an horizontal tube furnace (900 °C during 3 hours in a N₂ flux of 80 l/min and a heating speed of 10° C/min). After cooling to 100° C inside the furnace, the samples were introduced in a desiccator till reach the room temperature. In this conditions is determined the mass lost. This experiment was also carried out with 2.5 g of powder graphite (60-100 μm). Taking into account that the hydrogen content of graphite must be very small, the first assay performed was the mass loss of relatively large amount of graphite by volatile material release

when it is heating. Additionally the sample must have in powder in order to facilitate the volatile release.

2.5 g of powder samples (60-100 μm) of R and C graphite were heating at 900° C in inert atmosphere, detecting a small amount of mass loss in the order of 0.20 % in R graphite and 0.18 % in graphite C.

4.2.1.3 Controlled Thermal Desorption-IR spectrometry analysis [15]

The controlled thermal decomposition were carried out on powder samples in a furnace LECO that allows to maintain a pre-programmed slope of heating between room temperature and 1500° C. The released gasses are analyzed by IR spectrometry that allows determining the CO₂ and H₂O generated in the treatment. The furnace can be maintain at different atmospheres inert (N₂) and oxidizing (O₂). When the atmosphere is inert only is detected the water content and the CO₂ absorbed in the graphite (probably some amounts from the reaction of the O₂ absorbed with the carbon of the structure). When the atmosphere is oxidizing CO₂ and H₂O resulted from the oxidation of the extracted molecules.

By this procedure is detected:

- In Inert atmosphere till 1000° C, CO₂ and H₂O absorbed as gasses.
- In oxygen atmosphere till 450°C hydrocarbon compounds
- In oxygen atmosphere >450° C, free H₂ or undefined bounded (probably bonded in a hydrocarbon molecule).

The analyses in N₂ inert atmosphere (Figure 4.4) showed a peak that corresponds to the water release between 20 and 120° C. Water release at higher temperatures decrease and stay constant.

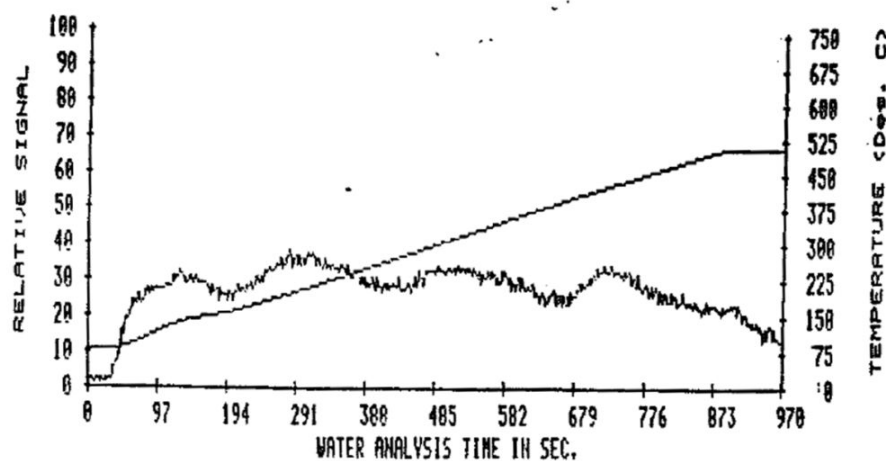


Figure 4.4 Thermo-desorption in N₂ atmosphere

The simultaneous analysis of CO₂ detect a release in coincident with water release. The CO₂ release can be originated from CO₂ adsorbed in the surface or by adsorbed O₂ that reacts at high temperature.

The oxygen analyses to fraction the hydrocarbon compounds desorption were carried out increasing the temperature in four slopes between 20° C and 500° C (Figures 4.5 and 4.6)

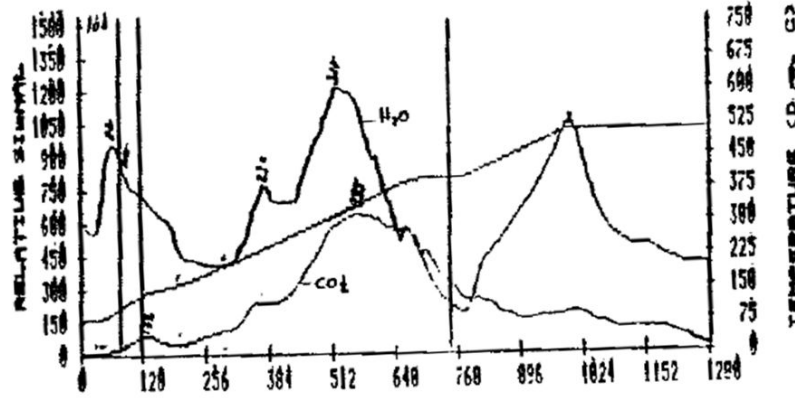


Figure 4.5 Thermo-desorption in O₂ atmosphere.
IR analysis of pyrolysis of graphite C

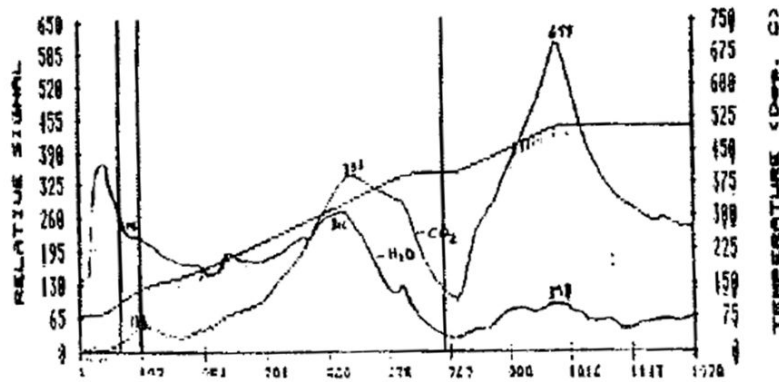


Figure 4.6 Thermo-desorption in O₂ atmosphere.
IR analysis of pyrolysis of graphite R

The C/H ratios in the two first slopes are under the hydrocarbon compounds (Table 4.2, that could be caused by the existence of adsorbed H₂O). In the third slope (130-300°C) C/H ratio increases which corresponds to saturated hydrocarbon compounds with 2-4 C atoms. However, desorption temperatures are higher than boiling points of this substances that could be caused by the vapour pressure increment by pore system location of this compounds. On the other hand it is possible that another hydrocarbon compounds with higher C/H ratio were release and the signal were hiding below the low C/H signal.

Table 4.2 C/H ratio in the products released by Thermal Desorption

Temperature Range	C/H Ratio	
	C Graphite	R Graphite
0-100	0.030	0.02
100-130	0.110	0.20
130-450	1.003	0.98

It is observed, analysing in detail the Figures 4.4 and 4.5, that there are a specific desorptions at 130-133°C, 200-230°C and 300-330°C. Also is observed that carbon content in the hydrocarbon compounds desorption increase when the temperature is higher than 330°C.

It is deduced the existence of light hydrocarbon molecules that are released in a wide temperature range depending on the pore size and possible existence of heavier hydrocarbon compounds which are released at temperatures higher than 300°C.

4.2.1.4 Pyrolysis flash

Very high heating speed experiences (Pyrolysis flash) were performed. Approximately 2 mg of graphite R were introduce in a Pyro-probe 1000, that allows heating the sample, by mean of a platinum probe, to 900° C in a fast way (20°C/ms), being practically instant the gasses released. The composition and the amount of hydrocarbon molecules had been determined by chromatograph Shimadzu GC-14A with flame detector.

Pyrolysis flash was performed in order to concentrate the volatile material out-put. The analysis of the produced gasses is expressed in weight% in Table 4.3. The expected uncertainty values are high due to the experimental set-up.

Table 4.3 Hydrocarbons detected in the graphite pyrolysis by Gas Chromatography

Hydrocarbon Compound	Detected weight %
Methane	0.028
Ethylene/Acetylene	0.0055
Ethane	0.0052
Propylene	0.0043
Propane	0.0014
2-methy-propane	0.0033
Butylene/Butene	0.0027
TOTAL	0.05

It is remarkable the presence of light hydrocarbon compounds, especially methane that is double concentrate that the other detected compounds, and the concentration in the gas release is higher as the molecular weight is lower. The total fraction of released hydrocarbon compounds is calculated around 0.05%. The difference till 0.2% detected for graphite R is possibly due to the presence of CO, CO₂ and H₂O non detectable by flame detector.

4.2.1.5 Controlled Thermal Desorption- GC-MS (17)

This procedure was used for determined the compounds released under 300° C.

It was used a ATD-400 Perkin-Elmer apparatus with a desorption time of 5 minutes at 300° C. The extracted products are analysed quantitatively by Gas-Chromatography with a FID detector and MS in a 30-300 uma range.

The attempt to identify the desorbed products by GC_MS of the gasses produced in the controlled thermal desorption (till 300°C) of powder Vandellós 1 virgin graphite detecting smilar products than in the pyrolysis assay.

4.2.1.6 Thermo-gravimetry (TG) and Differential Scan Calorimetry (DSC)-IR Spectrometry

A quantitative study by thermo-gravimetry was performed once was checked the presence of volatile hydrogenated compounds by IR spectrometry.

The equipment used was Metler TG-50 and DSC-25 controlled by microprocessor TC-11. Data analysis was done by Graphware TA72.2/5. Samples used were standard powder (0.63 and 0.100 mm) and 8x6x4 blocks standardized from virgin sleeves of Vandellós 1.

4.2.2 Solvent Extraction

The difficulties encountered to desorbed substances at temperature higher than 45° C in oxidising atmosphere are caused by the previous combustion of graphite and the impossibility of their detection by GC-MS if is performed in an inert atmosphere due to the thermal limits of the chromatographic column drives to design a concentration step by solvent extraction.

Extractions with S₂C were performed In a Soxhlet system during 24 hours from 20 g of graphite powder sample (60-120 μm) and the extraction products were analysed in a Gas Chromatograph system HP-5890.

Some samples were exposed at ambient before extraction in order to check the adsorption of volatile organic compounds.

Extracting The organic compounds with S₂C heavier molecules are detected than in the other methods (Table 4.4) due to it is not an aggressive treatment that avoid bonds breaking.

Table 4.4 Hydrocarbons detected by Gas Chromatography after extraction with S₂C

Hydrocarbon Compound	% relative
1-3 dimethyl nonane Benzene,	2.93
1-phentyl Ethanone	10.4
2-methyl Benzaldehyde	25.62
4-methyl Benzenemethanol	2.67
1-ethyl-4-(1-methyethyl) Benzene	5.91
1-3 dimethyl-5-(1methilet) Benzene	10.14
1-4 dimethyl-2-(1methilet) Benzene	14.69

4.3 Inventory determination of Sleeves of Vandellós 1

It was performed the following radiochemical determinations:

- Gamma Spectrometry direct measurement of massive and powder samples
- H-3 and C-14 by catalytic combustion furnace of powder graphite
- Beta-gamma, pure beta and alpha emitters over dissolved powder samples of T5

Table 4.5 Specific activity (Bq/g) of cuts of sleeve 1 powder samples

Sample	H-3	C-14	Co-60	Cs-137	Cs-134	Mn-54	Zn-65
1T	1.535	16.539	795	54	10	66	92
2T	1.739	15.873	717	32	--	69	61
3T	2.634	15.540	621	67	--	45	69
4T	1.857	15.281	706	45	--	71	71
5T	1.546	14.985	740	171	14	59	84
6T	1.739	15.170	747	49	--	72	69

1-2A	3.015	17.057	888	111	--	--	--
5A	1.591	14.134	769	190	14	56	55
6A	2.582	16.280	1054	102	--	77	10
Up-inner	10.360	34.151	14.837	1.887	144	110	--

Table 4.6 Specific activity (Bq/g) of cuts of sleeve 2 powder samples

Sample	H-3	C-14	Co-60	Cs-137	Cs-134	Mn-54	Zn-65
1T	35631	15392	6.808	32	1.398	84	--
2T	34184	14504	4.958	703	1.584	106	--
3T	32301	14282	4.366	51	1.217	83	--
4T	39960	9731	4.292	61	1.154	58	--
5T	50690	14282	4.140	22	11.026	57	--
6T	52170	14060	4.218	18	1.124	--	--
1-2A	32486	14615	3.922	37	943	77	93
5A	39590	13172	3.774	37	1.039	--	--
6A	50320	13172	3.496	14	1.013	56	--

Table 4.7 Specific activity (Bq/g) of cuts of sleeve 3 powder samples

Sample	H-3	C-14	Co-60	Cs-137	Cs-134	Mn-54	Zn-65	Eu-155	Na-22
1T	82700	4060	5.360	523	--	--	--	--	--
2T	134000	410	6.860	533	--	--	--	--	--
3T	187000	4160	8.260	488	--	--	--	51	39
4T	242000	4150	10.100	518	--	--	--	78	28
5T	388000	4270	11.600	511	--	--	--	55	48
6T	310000	3890	73.30	295	--	23	--	29	21
1A	76400	4070	--	--	23	--	--	--	--
2A	112000	3950	--	--	--	--	--	--	--
5A	231000	3880	--	--	--	--	--	--	--
Up-inner	76800	14400	--	--	199	--	--	--	--
Up-outer	70400	9170	--	--	--	--	--	--	--

Table 4.8 Specific activity (Bq/g) of pieces from sleeves 1 and 2

Sleeve	Sample	Mass (g)	Co-60	Cs-137	Cs-134	Mn-54	Zn-65	Co-57
1	11-24	674.3	699	89	15	48	78	--
	3	683.6	928	48	16	89	98	--
	4	675.6	921	60	20	68	100	--
2	11-24	652	54760	39	1690	68	85	30
	3	663.1	73630	3	2338	106	136	36
	4	691.3	71040	48	2301	98	122	42

Table 4.8 Specific activity (Bq/g) of dissolved powder of 5T

Nuclide	Sleeve - 1	Sleeve -2
Co-60	920	4477
Cs-134	182	46
Cs-137	13	120
Mn-54	60	59
Zn-65	72	93

Co-57	4	19
Cd-109	34	40
K-40	123	136
Na-22	1.5	12
Xe-133	1.9	13
Sr-total	48	28
Ce-144	11	--
Eu-155	--	38
Gross alpha	11	18
Am-241	7	8
Th-234	30	--
U-235	2	--

4.4 Inventory determination of Moderator of Vandellós 1

4.4.1 Determination of Tritium and Carbon-14

Samples of graphite powder were placed into a combustion oven where the sample combusts in a stream of oxygen gas at 900°C, it then passes the combustion products through a series of ceramic materials at 680°C that trap the volatile beta-gamma emitters present in the sample. Metals, salts and materials with very high melting points remain in the boat. The gaseous sample is passed through a section of teflon tubing where most of the $^3\text{H}_2\text{O}$ vapour condenses on the walls. The gaseous products are then passed through a vial containing tritium trapping scintillation solution where the remaining $^3\text{H}_2\text{O}$ vapour is condensed and trapped. The tritiated water droplets remaining on the walls of the teflon tubing are then washed down into the vial with tritium trapping scintillation solution.

$^{14}\text{CO}_2$ passes through the tritium vial without reacting with the tritium trapping scintillation solution. The gas is then bubbled through the vial containing carbon trapping scintillation solution where it reacts almost instantaneously with the solution. Both vials are then purged with nitrogen to carry off any free oxygen that will produce a reduction in counting efficiency due to chemical quenching. Samples are then ready to be counted by liquid scintillation counting.

4.4.2 Determination of High Energy γ -EMITTERS

High-energy γ -emitters were determined by direct high-energy γ -spectrometry, without radiochemical separations, using a conventional system that consists of a MCA S-35 from Camberra System and a coaxial HPGe detector with relative efficiency 20%. Spectra were analysed using Spectran-AT program and the efficiency curves for the specific counting geometry were obtained with a QCY-48 standard solution from Amersham.

Some radionuclides such as ^{59}Fe and ^{94}Nb , need a specific radiochemical separation process, prior to their determination by γ -spectrometry although they are high-energy

γ -emitters. The radioactive concentration of these nuclides in the samples was some orders of magnitude less than the concentration of the other β - γ emitters whose emissions disguise ^{59}Fe and ^{94}Nb lines [16,17]. The radiochemical separation of ^{59}Fe is described together with ^{55}Fe and the separation process of Nb is described below.

Niobium-93m/94. The radiochemical separation procedure of niobium is based on its selective precipitation as Nb_2O_5 in 4M HCl medium after addition of known amounts of stable Nb(V) as carrier. The precipitate Nb_2O_5 is dissolved by HF, forming the stable complex NbOF_5^{2-} . The chemical yield of the separation process is obtained by spectrophotometric measurements of the stable purple complex Nb-PAR. Then, ^{94}Nb and $^{93\text{m}}\text{Nb}$ were measured by high-energy and low-energy γ -spectrometry respectively.

4.4.3 Determination of Pure β and β - γ Emitters

In order to analyse the **non-volatile radionuclides** one aliquot of the original graphite powder sample was dissolved by an acid treatment with H_2SO_4 , HNO_3 and HClO_4 acid, obtaining a final solution that was prepared in order to obtain the solution in 4M HCl.

Iron-55/59. Ferric ions are precipitated as hydroxides by ammonia after addition of known amounts of stable iron as carrier. The precipitate is dissolved in concentrated nitric acid. The final solution obtained is 0.5M HNO_3 . The measured is carried out once the possible gamma interferences are checked by gamma spectrometry. ^{55}Fe is determined by liquid scintillation counting by the measured of Auger electrons which are consequence of radioactive decay by electron capture. ^{59}Fe is measured by gamma-ray spectrometry. The chemical yield is determined by spectrophotometry from the initial iron added as carrier.

Nickel-59/63. Nickel is precipitated with dimethylglyoxime, after addition of known amounts of stable nickel as carrier for determination of the chemical yield by spectrophotometry. A liquid-liquid extraction of nickel with chloroform and re-extraction with 0.5M HCl is carried out. The final solution obtained is 0.2M HCl. ^{63}Ni is determined by the measured of its beta emission by liquid scintillation counting once the possible gamma interferences are checked by gamma spectrometry. ^{59}Ni is measured by X ray spectrometry with a planar Ge detector..

Strontium-89/90. Strontium is separated by adsorption on an Eichrom Sr-Resin column after addition of known amounts of stable strontium as carrier and after conversion of the solution to the nitrate form. The resins are performed with 8M HNO_3 ., 8M HNO_3 -0.5M oxalic acid and 8M HNO_3 . The elution of strontium is carried out with 0.05M HNO_3 . The solution obtained is evaporated to dry, then it is added HNO_3 and again is evaporated to dry in order to be sure that all sample is in the nitrate form. Finally the residue is weighed and the weigh corresponding to $\text{Sr}(\text{NO}_3)_2$ form is obtained in order to determine recovery of carrier. $^{89/90}\text{Sr}$ is determined by the

measured of its beta emission by liquid scintillation counting once the possible gamma interferences are checked by gamma spectrometry. Two counting are made, one immediately after the separation and the other one with a minimum time interval of 8-10 days to correct the influence of ^{89}Sr .

Calcium-41/45. Calcium separation is based on selective precipitation reactions by hydroxides, carbonates and chromates after addition of known amounts of stable calcium. At the end of the radiochemical separation procedure the calcium carrier, together with the radionuclides of calcium, is precipitated as calcium carbonate, which is dried and weighed to determine recovery of carrier. Next, the precipitate is dissolved in hydrochloric medium in order to measure the Auger electron emissions, which are consequence of radioactive decay by electron capture, from ^{41}Ca and the beta emissions from ^{45}Ca . The measured is performed once the possible gamma interferences are checked by gamma spectrometry, by dual label measurement in a liquid scintillation counter.

Chlorine-36 (Volatile radionuclide). Chlorine separation is based in an oxidation technique performed in the graphite powder sample. The graphite sample is dissolved with HNO_3 , HClO_4 and H_2SO_4 acid. The gasses formed during the dissolution pass through a series of NaOH bottles where chlorine (^{36}Cl) and carbon dioxide (^{14}C) are trapped. The basic solution obtained is neutralised in order to measure the ^{36}Cl beta emissions by liquid scintillation counting. The measured is carried out by the dual label technique.

4.4.4 Determination of α -Emitters

The determination by alpha spectrometry requires the separation of the α -emitters from fission products, rare-earth and other elements that interfere in the preparation of the radioactive source and its measurement. All alpha emitters sources are prepared by electro-deposition and measured by a 450 mm^2 ion implanted silicon detector

Plutonium. The separation of plutonium is performed by anion exchange chromatography. Fission products and rare-earth are eliminated washing the column with nitric-methanol. Americium and curium are eluted with HNO_3 and finally, the column is rinsed with HCl solution and plutonium is eluted with HCl/HI solution. To calculate the chemical recovery, ^{242}Pu is used as tracer.

Americium and Curium. The solution of americium and curium, obtained in the separation of plutonium, are extracted with 0.45M Di(2-ethylhexyl)phosphoric acid in n-heptane. Americium and curium are reextracted with HCl . Finally, americium and curium are purified by anion exchange chromatography. To calculate the chemical recovery, ^{243}Am is used as tracer.

Uranium. The separation of uranium from plutonium, americium, curium, rare earth and fission products is carried out by liquid-liquid extraction with TBP-n-heptane. Uranium is extracted and purified by anion exchange chromatography. To calculate the chemical recovery ^{232}U is used as tracer.

4.4.5 Results

For the first step of characterisation some gamma emitters determined by direct γ spectrometry shown all values under minimum detectable activity (MDA): ^{24}Na , ^{54}Mn , ^{58}Co , ^{59}Fe , ^{65}Zn , ^{95}Zr , ^{106}Ru , $^{108\text{m}}\text{Ag}$, $^{110\text{m}}\text{Ag}$, ^{125}Sb , ^{144}Ce and ^{152}Eu .

The results of characterisation, in terms of maximum and minimum activity determined, average specific activity and their standard deviation as well as the ratio of data up to minimum detectable activity are collected in Table 4.9.

Specific activity variation in function of height from the pile base and approximately distance from the pile centre in each vertical section is plotted in figures 4.7 to 4.10 for ^3H , ^{14}C , ^{60}Co and ^{137}Cs . Data from double sample at the same position (same distance to the centre and height) are represented as average value of specific activity.

Table 4.9 Ranges of specific activity (Bq/g) up to MDA from nuclides determination at 1st Characterisation step

	> MDA (%)	Maximum (Bq/g)	Minimum (Bq/g)	Average (Bq/g)	STD (%)
^3H	100.0	1.69E+06	2.30E+04	3.57E+05	79.3
^{14}C	100.0	1.56E+05	8.54E+03	7.10E+04	54.5
^{22}Na	65.5	7.45E+02	3.24E+01	2.19E+02	73.9
^{60}Co	100.0	9.79E+04	1.25E+02	2.08E+04	108.0
^{94}Nb	6.9	1.65E+02	2.38E+01	7.77E+01	70.5
^{133}Ba	62.1	1.01E+03	3.34E+01	3.28E+02	73.2
^{134}Cs	50.0	1.18E+03	6.09E+01	3.00E+02	67.7
^{137}Cs	44.0	3.83E+03	1.33E+01	4.20E+02	179.7
^{154}Eu	22.0	1.76E+03	2.64E+02	7.54E+02	51.6
^{155}Eu	35.0	7.15E+02	9.27E+00	2.17E+02	66.7
^{241}Am	26.0	1.04E+02	3.30E+00	2.33E+01	94.5

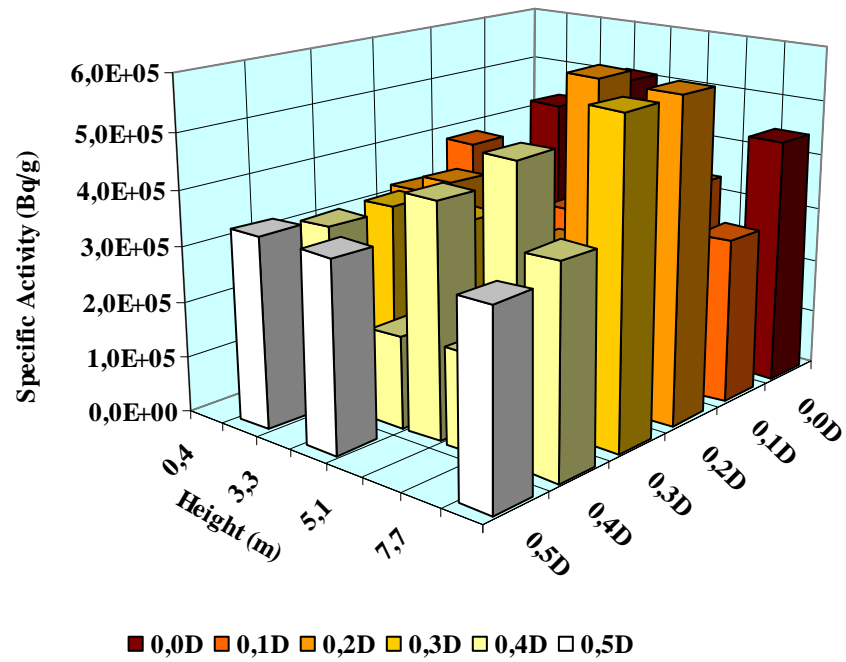


Figure 4.7 ³H specific activity distribution

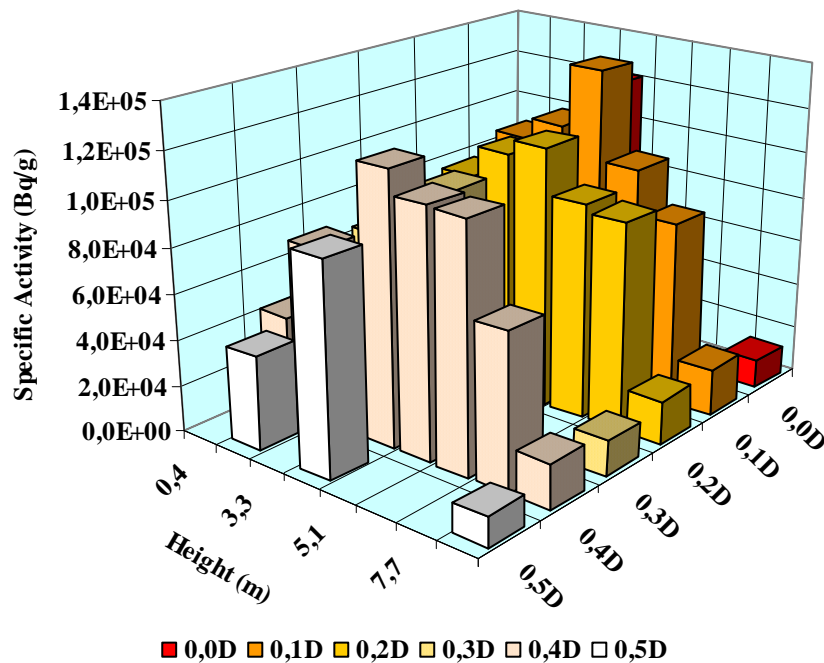


Figure 4.8 ¹⁴C Specific activity distribution

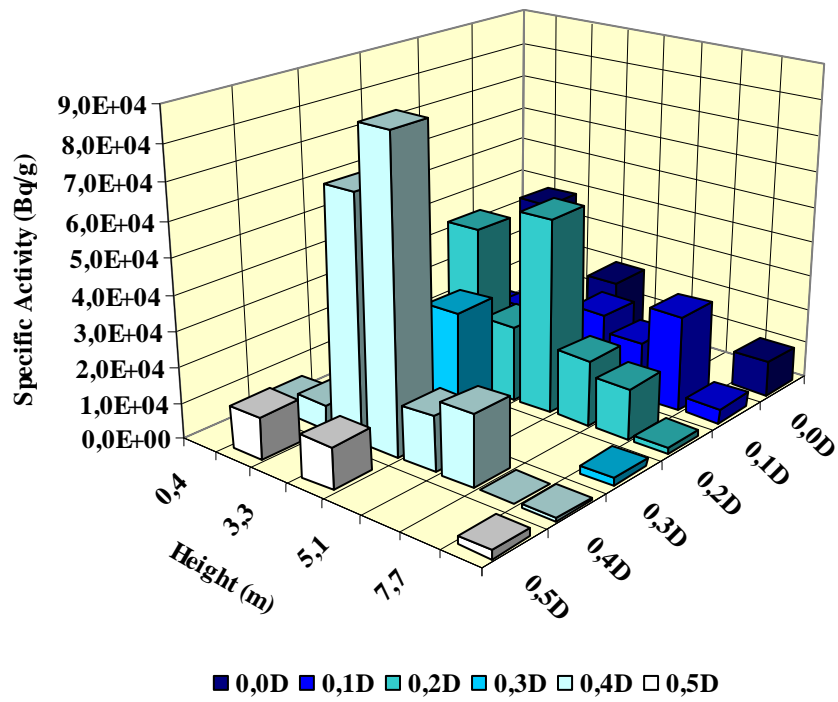


Figure 4.9 ⁶⁰Co Specific activity distribution

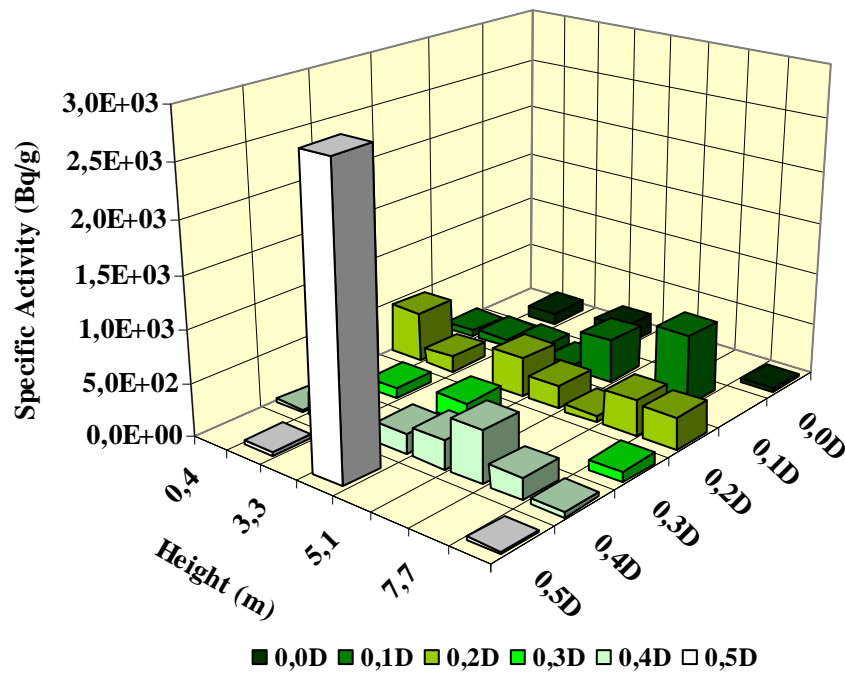


Figure 4.10 ¹³⁷Cs Specific activity

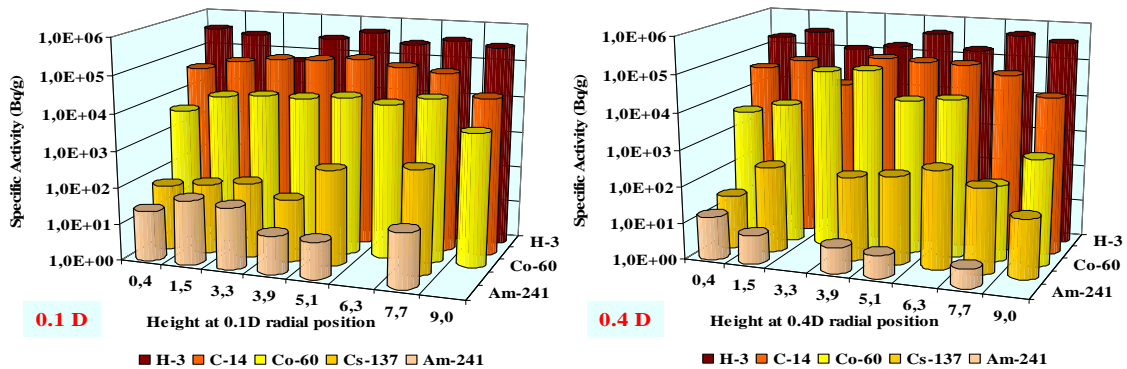


Figure 4.11. Distribution of specific activity of main nuclides in function of pile height at the radial 0.1D and 0.4D positions.

The evolution of activity along two vertical lines (0.1 D and 0.4 D) are represented in figure 4.11 for the main 5 nuclides (³H, ¹⁴C, ⁶⁰Co, ¹³⁷Cs and ²⁴¹Am).

The same representation for samples taken at two pile heights (3.9 m and 9.0 m) along the radius is shown in figure 4.12.

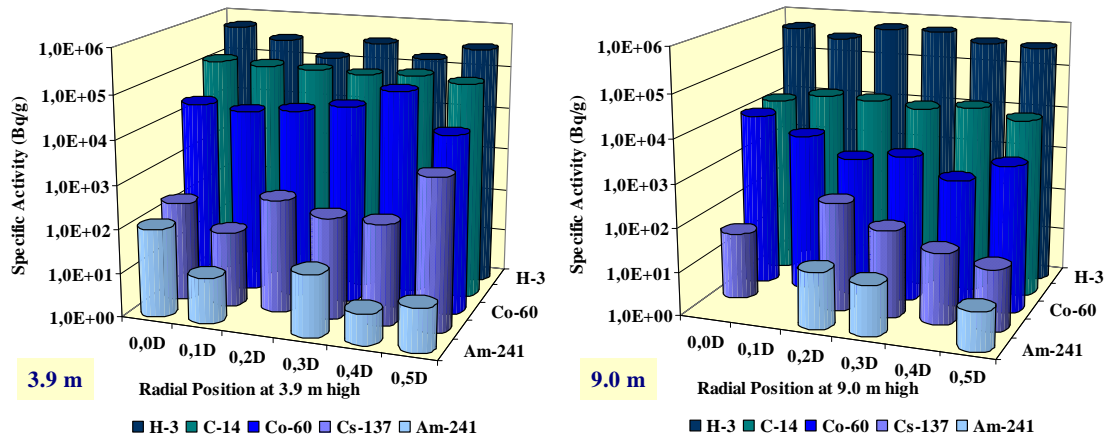


Figure 4.12. Distribution of specific activity of main nuclides along the radius at: 3.9 and 9.0 m height.

Six samples were selected for performing the second step characterisation process. These samples were G-5, G-13, G-16, G-23, G-30 and G-37.

The specific activity determined for ^{36}Cl , ^{59}Fe , ^{59}Ni , $^{93\text{m}}\text{Nb}$ and ^{94}Nb are under minimum detectable activity. Maximum, minimum and average specific activity of the six samples and the ratio of the data considered for calculations are collected in Table 4.10.

The same parameters for the nuclides of the first step of characterisation in these six samples are collected in Table 4.11.

Table 4.10 Ranges of specific activity (Bq/g) up to MDA of nuclides determined at 2nd Characterisation step

	> MDA (%)	Maximum (Bq/g)	Minimum (Bq/g)	Average (Bq/g)	STD (%)
^{41}Ca	100.0	4.65E+02	7.06E+01	2.04E+02	63.9
^{55}Fe	100.0	1.56E+04	1.34E+03	7.83E+03	70.3
^{63}Ni	100.0	3.28E+04	1.25E+03	1.43E+04	84.5
^{89}Sr	100.0	1.04E-01	1.04E-02	3.86E-02	87.6
^{90}Sr	100.0	7.65E+02	7.04E+01	2.60E+02	97.0
^{238}Pu	100.0	1.31E+02	6.44E+00	4.47E+01	92.0
$^{239/40}\text{Pu}$	100.0	2.06E+01	3.53E+00	8.79E+00	65.0
^{241}Pu	100.0	1.94E+03	2.87E+02	7.21E+02	79.3
^{241}Am	100.0	6.40E+01	1.33E+01	2.60E+01	68.5
^{242}Cm	100.0	6.10E-02	6.93E-03	2.90E-02	73.1
^{244}Cm	100.0	5.79E+02	1.75E-01	1.60E+02	134.6
^{234}U	100.0	2.42E+00	5.64E-02	7.90E-01	101.7

²³⁸ U	100.0	2.31E+00	5.90E-02	7.10E-01	106.6
------------------	-------	----------	----------	----------	-------

Table 4.11 Ranges of specific activity (Bq/g) up to MDA on six selected samples of nuclides determined at 1st Characterisation step

	> MDA (%)	Maximum (Bq/g)	Minimum (Bq/g)	Average (Bq/g)	STD (%)
³ H	100.0	5.11E+05	4.76E+04	2.78E+05	62.5
¹⁴ C	100.0	1.22E+05	1.99E+04	7.15E+04	46.9
²² Na	100.0	7.45E+02	1.43E+02	3.99E+02	57.1
⁶⁰ Co	100.0	4.36E+04	1.59E+03	1.62E+04	87.0
⁹⁴ Nb	33.3	8.26E+01	2.38E+01	5.32E+01	55.3
¹³³ Ba	83.3	1.01E+03	1.31E+02	5.47E+02	59.4
¹³⁴ Cs	100.0	7.12E+02	6.09E+01	3.57E+02	56.0
¹³⁷ Cs	100.0	3.83E+03	3.05E+02	1.42E+03	89.6
¹⁵⁴ Eu	83.3	1.76E+03	5.20E+02	1.11E+03	43.3
¹⁵⁵ Eu	100.0	7.15E+02	2.26E+02	4.00E+02	41.4

Relative activity of alpha, pure beta and beta-gamma emitters are plotted in bar diagrams as are shown in figures 4.12,4.13 and 4.14 respectively. The relative specific activity per nuclide is calculated as the ratio between activity of each sample and average activity of the six samples in order to get comparable activities values to study the tendency.

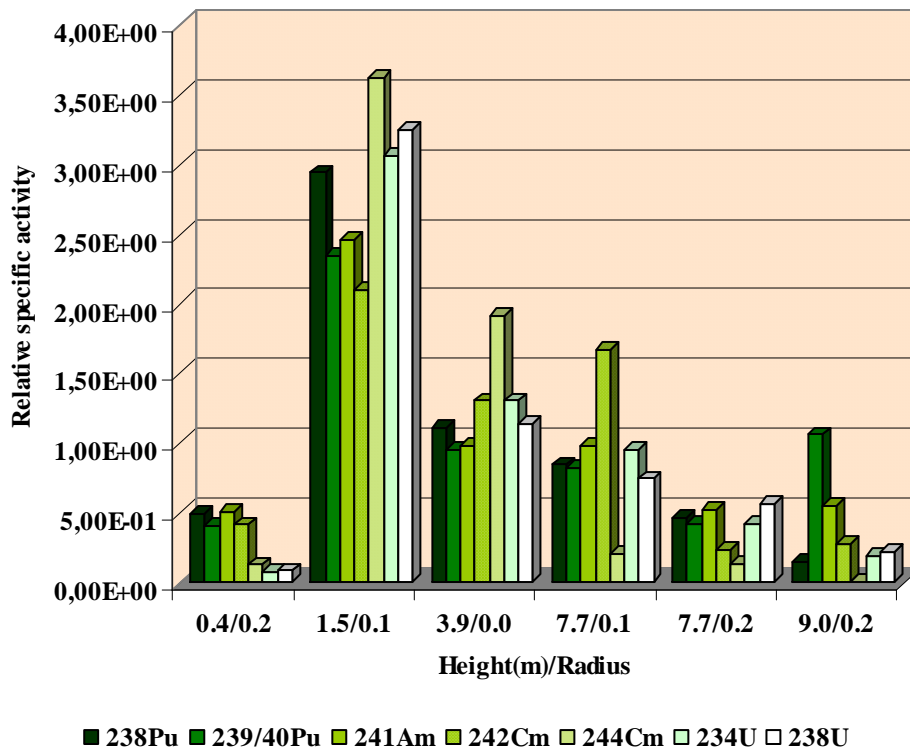


Figure 4.13 Evolution of alpha emitters

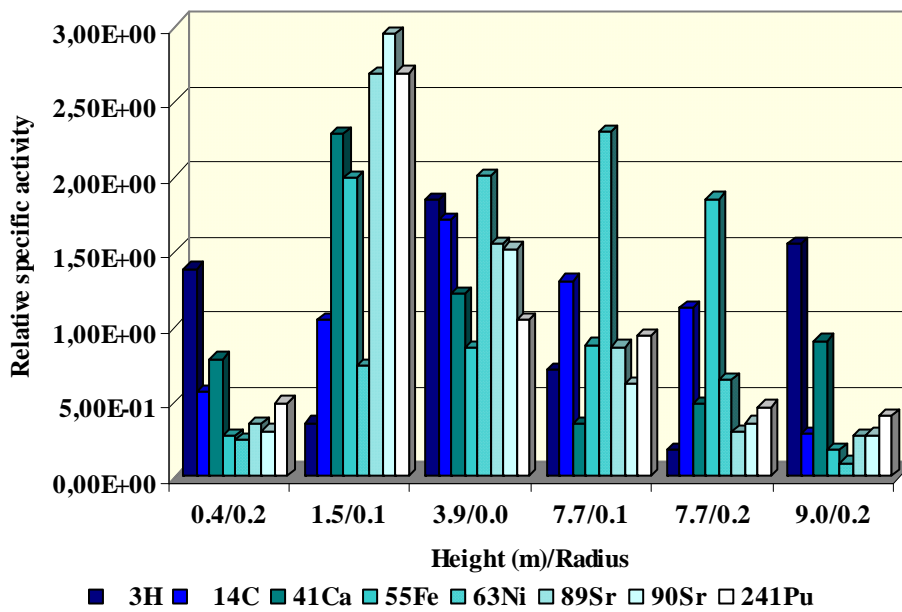


Figure 14 Evolution of pure beta emitters

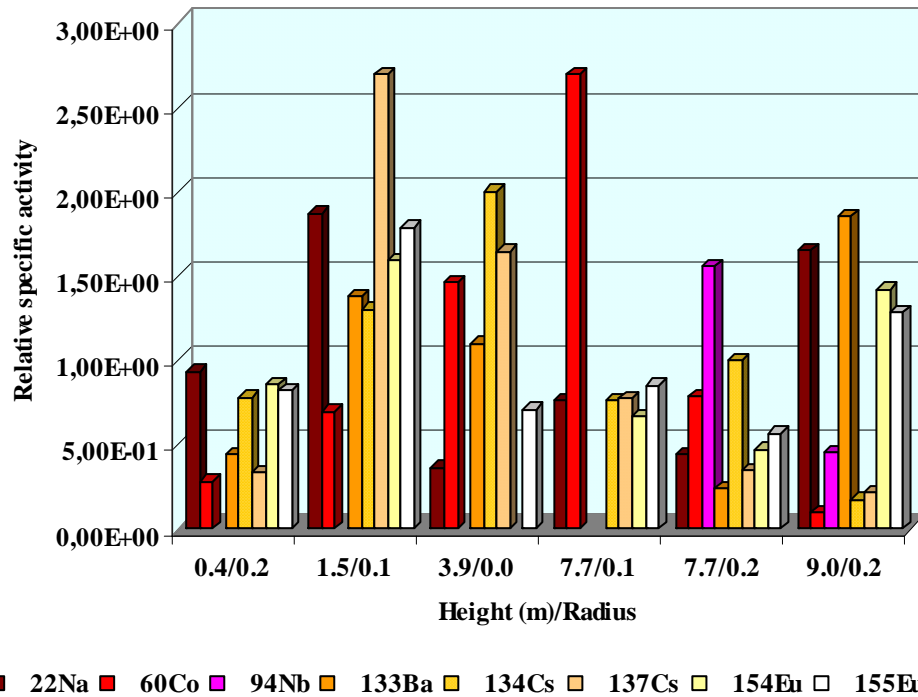


Figure 15 Evolution of beta-gamma

4.4.6 Discussion

The procedures applied for characterising the graphite samples are already implemented in the routine operation of the Waste Characterisation Project in CIEMAT as for other operational waste streams, however the special physico-chemical characteristics of graphite implied to apply a specific sample preparation process.

These processes are:

- Milling the graphite cylinders avoiding dispersion as well as contamination
- Homogeneous distribution of the obtained powder in order to fix a measurement geometry with adequate characteristics according to the standards for gross alpha-beta measurement and direct high energy gamma spectrometry.

Results from characterisation (Table 4.9) show some important direct conclusions:

Tritium activity appears as the higher radioactive nuclide in the graphite (around 10^5 Bq/g in average) that means one order of magnitude higher than the other two majority components ^{14}C and ^{60}Co . This could be produced by the activation of ^1H and ^2H bonded to the organic molecules associated at graphite and minor contribution from contamination coming from fuel during operation. Distribution of ^3H in figure 4.7 looks heterogeneous (Std $\approx 79\%$) regarding to both radial and vertical positions in the pile and presents higher activity concentration at height up to 7.7 and radial position in the range 0.2D to 0.1 D.

Activity of ^{14}C shows (figure 2) pretty regular trend distribution along the pile radius and a maximum concentration between 3.3 to 5.1 m height (central zone of the pile). Production of ^{14}C comes from activation of ^{12}C and being this nuclide the structural component of the pile, its concentration should be linked to the integrated neutron flux in each zone.

It is important to pay attention on the behaviour of activity ratio $^3\text{H}/^{14}\text{C}$ regarding to ^{14}C concentration. It is observed that as much as ^{14}C concentration grows up the ratio decrease faster, that could be in relation with the degradation of the structure of the graphite by the integrated neutron flux. When the structure is degraded there are more possibilities for ^3H to escape from the graphite structure and consequently reduce its activity. This behaviour was also observed in previous R+D works [18, 19] on leaching studies of graphite sleeves from the same plant when probes with higher activity concentration of ^3H presented lower leaching rates of ^3H .

Cobalt-60 present similar profile along the radius of the pile that ^{14}C with maximum activity concentrations in each radial distance at 3.3-3.9 m height. The maximum values were registered for 0.4D in opposition to the behaviour observed with ^{14}C in which the maximum concentration appears at lower radial distance. It is remarkable that the main source of ^{60}Co are the devices made of stainless steel wire used for fixing the fuel element into each graphite sleeve.

Cesium-137 activity distribution (figure 4.10) shows random distribution in both senses. so that we can conclude that its presence it is not in connection with the composition of the pile and neutron flux.

These distributions can be checked clearer in figure 4.11, where it is plotted the profile for five nuclides at radial positions 0.4D and 0.2D. It is possible to check the relation of activity concentration of these nuclides as well as the trend of ^{241}Am and ^{137}Cs that does not look in the same form that ^{14}C profile, so these nuclides are not correlated with integrated neutron dose. On the other hand the profile of ^{60}Co has the same tendency that ^{14}C . These remarks can be also checked in the profile of activity in function of radial position for 1.5m and 3.9 m height (Figure 4.12).

The study of activity distribution concerning the six selected samples for destructive characterisation shows that the activity concentration is higher in the samples that range from 1.5 m and 3.9 m height and no significant variance in function of the radial position of sample in the pile.

For alpha emitters the activity distribution presents the behaviour already mentioned for every nuclide tested (figure 4.13).

In the case of pure beta emitters (figure 4.14) besides of ^3H and ^{14}C all nuclides determined present practically the same tendency except for ^{63}Ni that presents a maximum at higher vertical level (7.7 m)

In the case of beta-gamma emitters characterised (figure 4.15) by direct measurement of the graphite powder, the behaviour is the same for every nuclide except for ^{137}Cs and ^{60}Co already discussed and ^{134}Cs whose tendency is the same than ^{137}Cs as was expected. We can also observe in these nuclides another local maximum in the sample collected at 9.0 m height.

5 CHARACTERISATION IN DECONTAMINATION STUDIES

The origin of the radionuclides in nuclear graphite before irradiation is by two mechanisms: Impurities activation or external contamination [20]. In the first case the impurities concentration and distribution leads to the concentration and location of activation nuclides, in the second case, for the sleeves getting by wet way, the contamination can be origin in the nucleus or by contamination by the water of the pool. In the sleeves by dry way or in the pile the contamination process is produced only in the nucleus.

A localised primary contamination In the nucleus is produced by punctual release from the fuel elements (from a micro fracture of the cladding) to the graphite sleeve and by secondary contamination transporting the nuclides through the cooling water from the same fractures.

A chemical interchange is produced between the graphite sleeves and the water when the sleeves are introduced in the pool. This interchange is holding in the pool till equilibrium is reached or till the sleeve is removed.

It seems that chemically it is found more chemical resistance to be removed in the activation products than in contamination products, due to in more cases the activation products are chemically bounded in the graphite structure and the accessibility of the extraction products is more difficult. In the second case the nuclides are adsorbed or chemisorbed in the surface layers where the extracting compounds can access or can extract by thermal treatment.

The studies try to determine the importance of these effects in the radioactive content in order to know their stability to predict the effectiveness of the treatments.

To characterise the reflector was analysed the radionuclides in the coolant and for the contamination in the pool several sleeves taking from the pool were analysed.

The contamination with metallic nuclides is more or less easy to assume but it was more difficult to find the tritium fixation in the matrix, being in the nucleus at more than 400°C it is remarkable the possibility to be adsorbed as gas. So that only can bounded, as protonated form, to molecules or specific graphite positions with free positions, that means less graphitised areas. The stability of tritium will be the ones of the molecules or positions were is bounded. To study it was used the thermal treatment and tritiation processes of virgin graphite as gas (TH) and water (THO).

On the other hand as is known tritium is transferred by isotopic interchanges among molecules that can lead to a release of tritium in the interchange with the environment humidity. For this the mechanism and kinetics of steam interchange were studied.

5.1 Kinetics and Mechanism of hydrocarbon adsorption-desorption

The existing hydrocarbons compounds are releasable by thermal treatment that was checking by IR-spectrometry as is described in 4.2.1. In order to check the presence of H-3 and C-14 in these release a more detailed study on characteristics of this release, stability of the compounds in the graphite, kinetics and thermodynamics of the adsorption-desorption by TG and DSC are performed [21]

5.1.1 Thermal treatment

A Mettler TG-50 and DSC-25 controlled by a microprocessor TC-11 was used in the analyses. The Software Graph Ware TA72.2/5 was used for data analysis. The samples were powder (0.63-0.10 mm) from Vandellós 1. The assays was performed following the data in Table 5.1

Table 5.1 Thermo-gravimetry and DSC on Vandellós 1 graphite

Sample	Temperature			Atmosphere		Type
	Initial (°C)	Final (°C)	Slope (°C/min)	gas	Cm ³ /min	
GVH30.1	25	900	30	He	20	TG
GVN16	30	1000	16	N ₂	20	TG
GVN01	30	540	1	N ₂	20	TG
GVA9	30	650	2	Air	St. cond.	DSC
GVA10	30	650	5	Air	St. cond.	DSC
GVA	30	650	10	Air	St. cond.	DSC
GVA13.1-8	30	650	10	Air	St. cond.	DSC

In every TG carried out a mass loss by products desorption is registered (Figure 5.1).

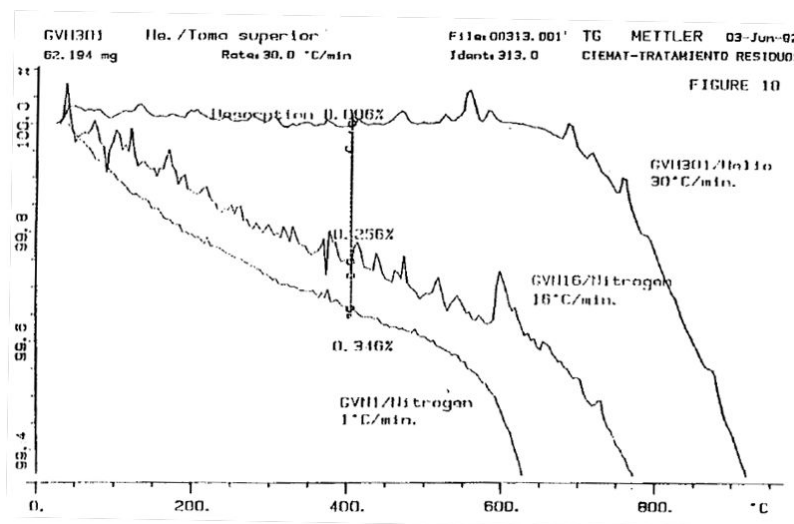


Figure 5.1 Thermo-gravimetry of graphite

The higher loss is produced at 200°C and is produced till 400°C where is reached the mass loss of 0.5%. Around 500°C the graphite corrosion starts being the mass loss continuing by combustion of C structure due to the oxygen impurities or the O₂ adsorption by the graphite. The desorption is time depending due to the slower slope implies higher losses (Fig 5.1 and 5.2)

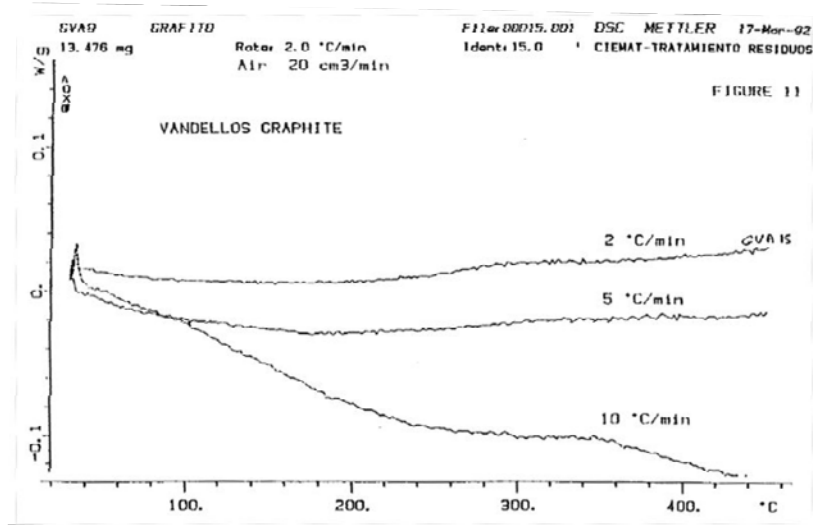


Figure 5.2 Thermo-gravimetry with different temperature slope

DSC spectra presents an endothermic process till 100°C or 175°C and exothermic from this temperatures. This behaviour can attributed to this temperatures are not enough to start the corrosion process. (Figure 5.3)

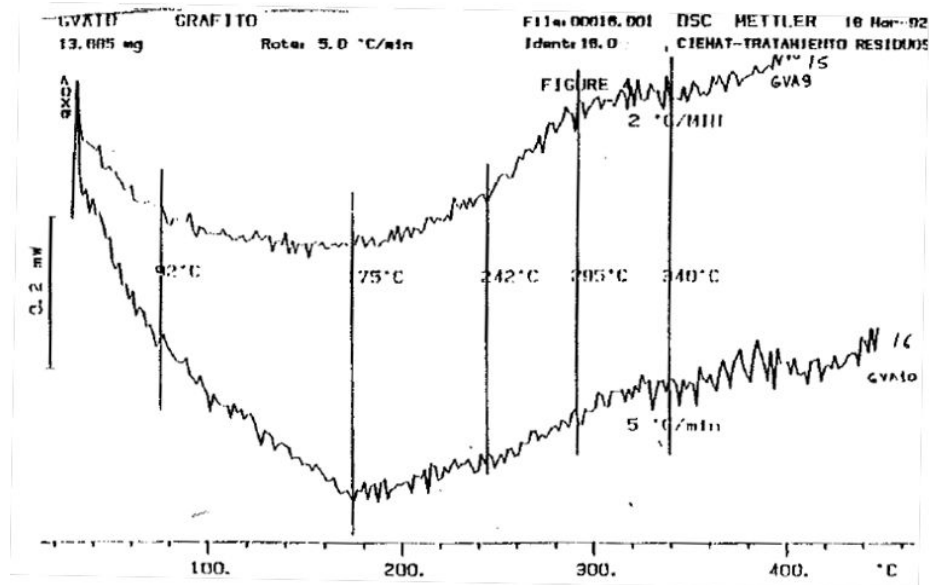


Figure 5.3 DSC of graphite samples

When is applied a desorption process over a sample already desorbed the release of hydrocarbon compounds increase (Figure 5.4). In a process repeated 8 times it is remarked an increment of products desorbed at low temperature. This demonstrate that the heating process promote internal reactions and generation of hydrocarbon compounds, probably in less graphitised areas, the temperature break the bnds with the structure and forms free hydrocarbon compounds.

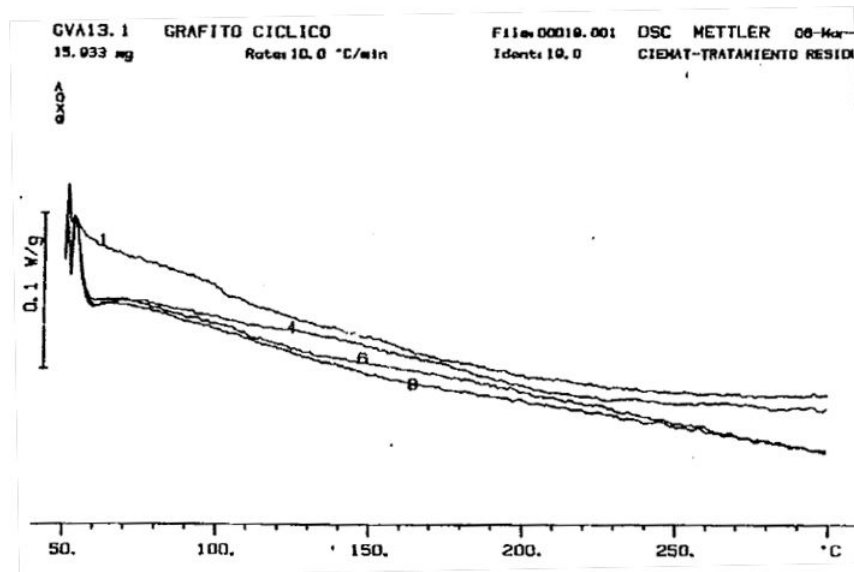


Figure 5.4 Consecutive Desorption processes of graphite

It has to take into account the need of an hydrogen source to form this compounds, as in reactor that contribute with a constant level of hydrogen from the cooling gas.

5.1.1.1 Desorption kinetics

An analysis of the desorption kinetics was allowed through TG and DSC curves. Correlation between desorption rate is given by:

$$\frac{d\alpha}{dt} = K \cdot (1 - \alpha)^n \text{ (Eq. 5.1)}$$

Where

α : Sample weight at time t / initial sample weight

t = time

K: rate constant that depends of temperature according to Arrhenius equation:

$$K = K_0 \cdot e^{-E/RT} \text{ (Eq. 5.2)}$$

The desorption kinetics was applied to 2 temperature ranges, from 25 to 400°C (The average work temperature of Vandellós 1) and another range >400°C.

Desorption in the range 25-400°C

Representing the desorption values from room temperature to 400°C (K vs 1/RT) it cannot find a singular lineal trend (Figure 5.5) that indicates the presence of several hydrocarbon compounds desorbed at the same time in the temperature range, so that there is not a singular kinetic process.

This can be caused by the formation of different products and different size pore location of the same product.

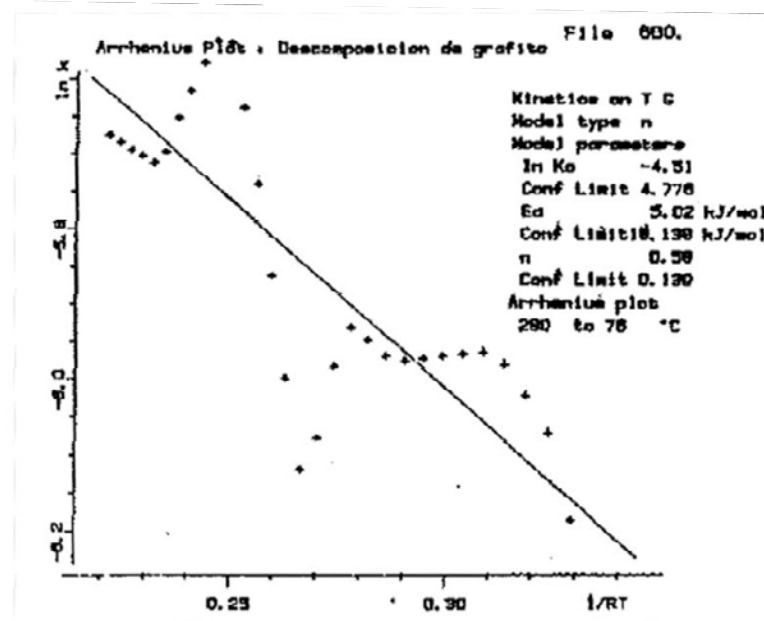


Figure 5.5 Arrhenius equation representation (K vs. 1/RT)

Desorption in the range 400-830°C

To determine desorption kinetics in this range a series of TG with a dynamic part and a isothermal part were performed (Figure 5.6)

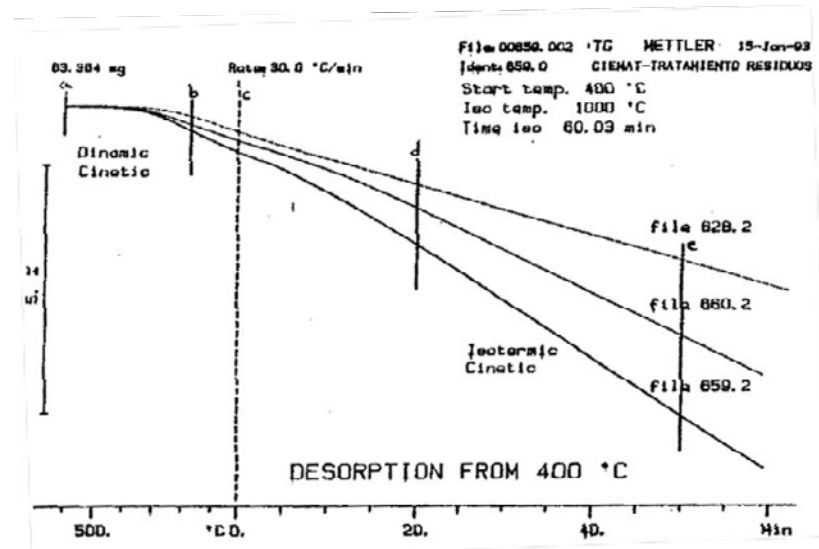


Figure 5.6 TG measurement to obtain data for adsorption kinetics

In this TG curves can distinguish 3 steps:

- Between a and b (till approx. 830°C) there is a kinetic represented by eq 5.1 and the Arrhenius representation shows the desorption of only one product Figure 5.7).
- Between b and d (from 830°C to 1000°C and ten minutes into the isothermal part) there is not a defined kinetic due to the juxtaposition of several phenomena.

- From d where the sample suffers a continuous mass loss there is an order zero kinetic in a linear shape.

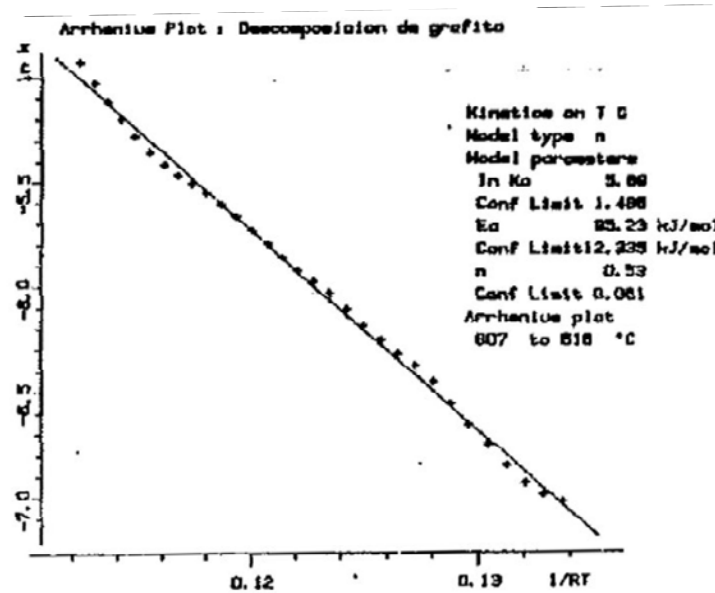


Figure 5.7 Kinetic constant representations for Arrhenius equation

5.1.2 Solvent Extraction

Benzene was used as radiocarbon model, due to that it is possible to find in graphite and is a probable product of a hydrogenation of graphite structure due to the presence of H₂ in the cooling gas.

Assays consists on immersion of a graphite block in benzene and desorbed by heating, checking the mass losses and the presence of other hydrocarbon derivates in the desorption products.

Higher amount of desorbed product is found than adsorbed product in consecutive benzene adsorption-desorption processes (Figure 5.8). This effect can be originated in the dissolution of other hydrocarbon compounds by benzene that are desorbed with it [22].

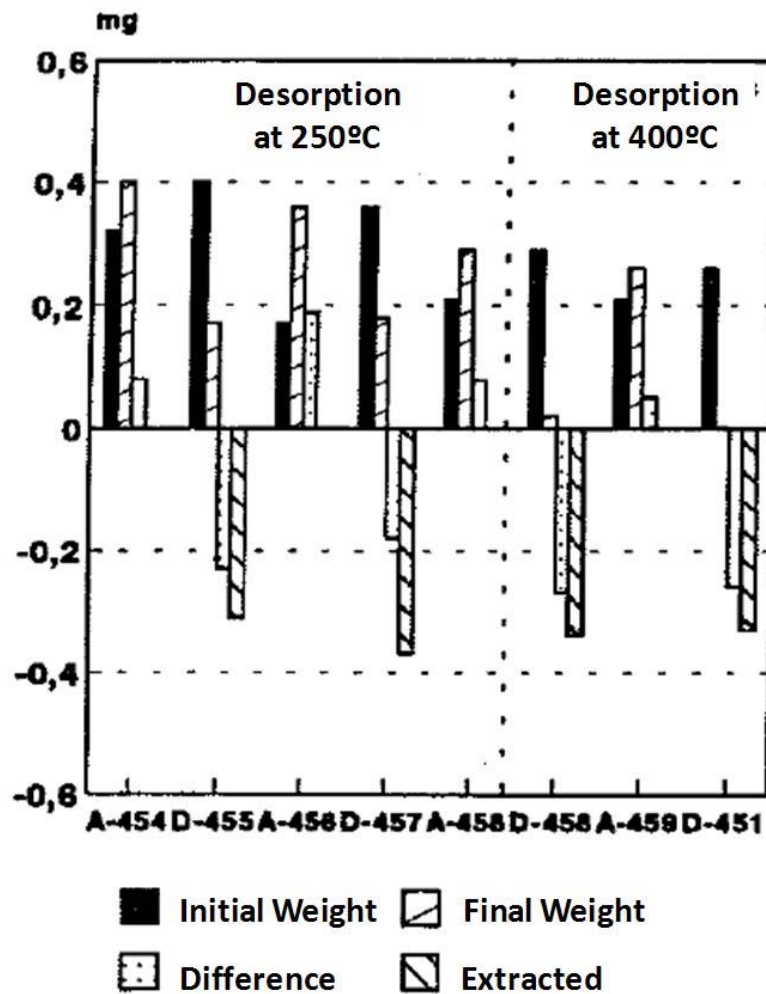


Figure 5.8

The phenomenon is similar to the observed with thermal treatment when hydrocarbon chains bounded to the structure break the bonds and release from the structure.

Nevertheless two different behaviours had been detected at 200°C and 400°C. In the first case adsorbed benzene in the first adsorption (Difference in A454) process extract all the product (Extract D455), that gives a space to be occupied by more adsorbed benzene.

In the second case it is extract all the product adsorbed in the first adsorption (D458) and in the second (D451) it was extracted even more than in the first.

In the second case not only has influence the solvent but the temperature. The more graphitised chains are released from the structure by effect of solvent and heating leaving space in the escape.

Finally it is demonstrated through the assays where promote the volatile compounds extraction by temperature or with joint effect of solvents and temperature that at low temperature it is extracted a little amount of this compounds. The desorption is much higher at temperatures $\geq 400^\circ\text{C}$ this desorption is higher but in these cases the corrosion of graphite is produced due to the adsorbed oxygen in the graphite surface.

5.2 Kinetic and Adsorption mechanism of water

To determine the kinetic parameters of water adsorption-desorption two consecutive experiments were done [23].

In the first one water was adsorbed on 4x4x6 mm graphite blocks in water saturated atmosphere at 27°C enough time to reach the equilibrium in order to obtain the corresponding constant.

In the second two types of desorption processes are performed in thermal-balance on the same samples, one isothermal at 25°C and other in a thermal range from 30 to 144°C with a temperature slope of 0.5°C/, in order to obtain desorption kinetics parameters.

The desorption data were obtaining by calculations from the equilibrium constant and desorption parameters.

5.2.1 Results and Discussion

Water desorption of water was performed in one of the two blocks in a isothermal mode at 25°C (Figure 5.9)

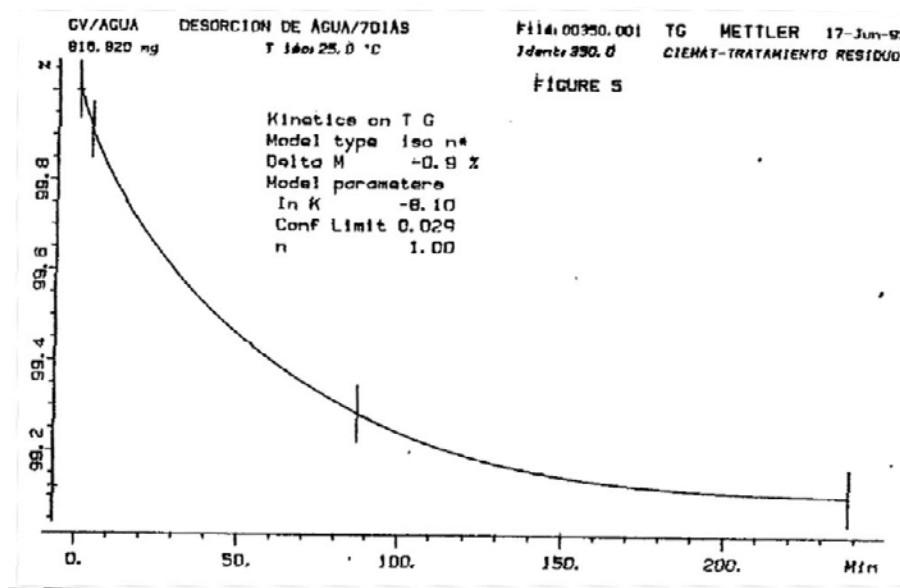


Figure 5.9 Isothermal Water desorption in graphite

The kinetics of this isothermal reaction is of order 1 following the equation

$$\frac{d\alpha}{dt} = K \cdot \alpha^n \text{ (Eq. 5.3)}$$

Where

α : Sample weight at time t / initial sample weight
t = time

K: rate constant that depends of temperature according to Arrhenius equation:

The rate and equilibrium constants at 25°C calculated are:

- $K = 3 \times 10^{-4}$
- $K_{eq} = 9 \times 10^{-3}$

The absorption rate can be calculated from this constants being 27×10^{-7} , factor 9000 lower than the desorption rate. This explains the difficulties to obtain the adsorption constants at temperatures higher than room temperature.

Adsorption and desorption variation versus time were calculate at 25°C from this data (Figure 5.10)

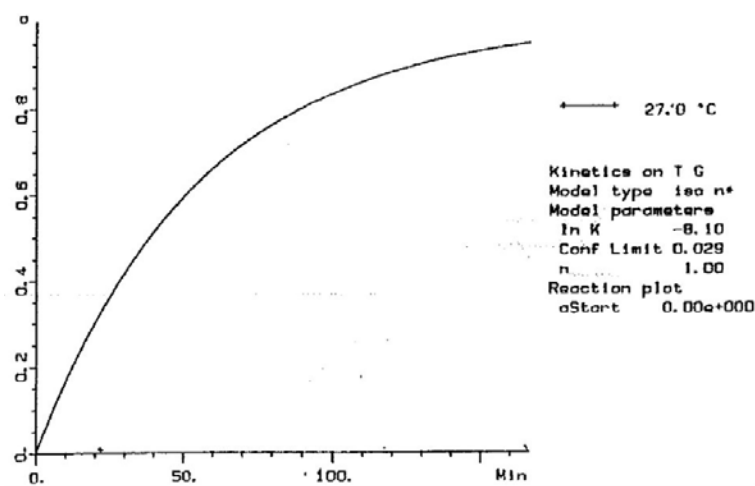


Figure 5.10 Water desorption in function of time in graphite

With the other bock desorption studies between 25°C and 150°C were performed (Figure 5.11)

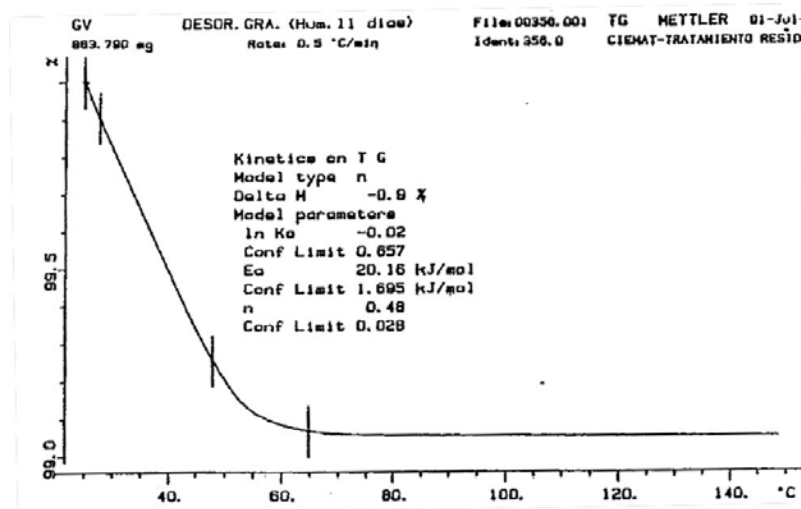


Figure 5.11 Water desorption in the range 25°C-150°C

Variation of the kinetic constant versus temperature can be obtained from the experimental data in agreement with Arrhenius equation (Eq.5.2).

Representing data K vs. $1/RT$ in the assay 356 (Figure 5.12) it can get the equation constants, where it can observe some pair values a slightly deviated from the trend that demonstrates the existence of several overlapping phenomena. Detailed analysis show several straights at different temperature range that could corresponds to several desorption process rates following different pore sizes.

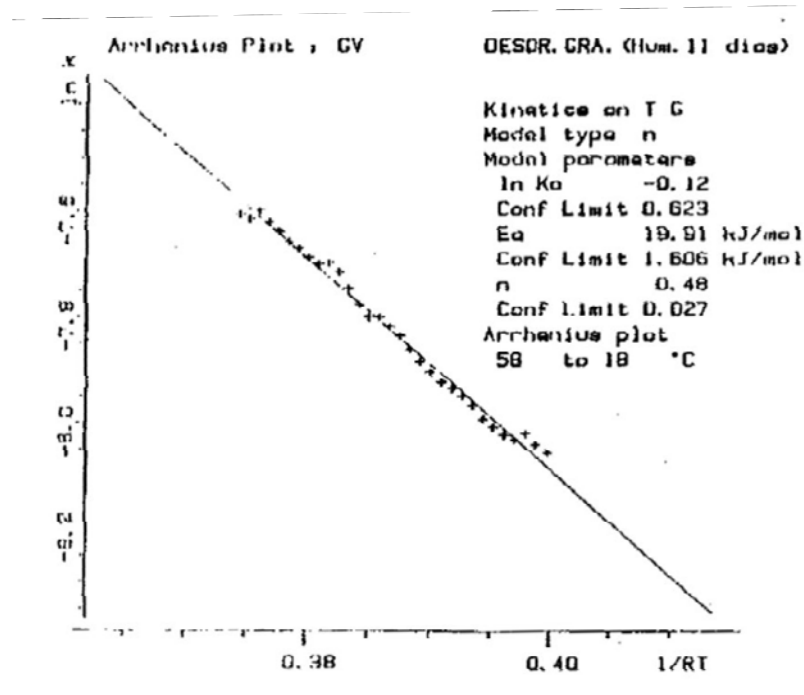


Figure 5.12 Arrhenius constant representation for water desorption

6 FINAL REMARKS

Graphite manufacturing, from mineralogical and agglomerate components, has an important role in their characteristics. In general terms graphite has a micro-crystalline structure together with more disorder areas irregular and with higher porosity.

The graphite from Vandellós-1 and JEN-1 has a relatively high homogeneity structure being their crystalline structure highly graphitisation degree.

The pores evaluated are in the range of macropores and mesopores with a high variety of sizes and shapes, No micropores were finding in the studies. The pore sizes and the number of pores is increased when the structure is treated with CO_2 increasing the macroporosity through the preference of CO_2 to the non mineralogical graphite, we guest that is the phenomenon could occur in the irradiation in the reactor.

The poly-cristaline structure, with disorder areas, lead to a properties with a high influence in the irradiated graphite behaviour. The pore surfaces control the adsorption properties of graphite and some of their contents.

The radioactive content depends on the storage in wet (reactor's pond) of the graphite, as happened with some fuel sleeves of Vandellós 1 graphite. The tritium content in this case is lower by nuclide interchange with water.

The inventory finding (ordered in decreasing activity concentration) is: ^3H , ^{14}C , ^{60}Co and ^{134}Cs being tritium some orders of magnitude higher than the others. In general the origin is the activation of the impurities and the C of the structure in the case of ^{14}C , although in some of the analysed graphite comes from contamination coming from the fuel-cladding fissure in a neighbour fuel element.

Tritium speciation in graphite is in the majority of cases as HTO, Hydrocarbons or HT that can be volatiles or taking part or non or less graphitised areas, as recently Carbowaste work on speciation was conclude [24].

Tritiated water is produced by mineral from environment than interchange tritium with surface layers of graphite. This water is release easily when the physical-chemical conditions are favourable

The accessibility of environment water (which is in thermodynamic equilibrium with graphite) to the pore system is fast at the beginning and very slow afterwards needed a long time of saturation. Nevertheless, the retained total amount of water is small.

The rest of tritium is chemical bonded to graphite structure, probably in free positions in the microcrystal edges or in the more disorder areas formed part of hydrocarbon products with a certainly degree of freedom regarding to the graphite structure.

The hydrocarbon compounds are stable at room temperature, but as the temperature is increasing the desorption of these is higher. Nevertheless, it is observed, at temperature higher than 400°C , carbon bonds breaking from less graphitised areas, together with desorption of hydrocarbons that drive to a generation of new hydrocarbon compounds.

Summarizing, the possibility of tritium release in gas form, as HTO from humidity interchange or -C-Tin volatile hydrocarbon compounds as well, at environmental condition in quantitative amounts is practicably negligible.

The radiocarbon is very stable, due to that in the majority of the case takes part of the structure being covalent bounded, even in the case that is in formed part of volatile hydrocarbon compounds it is needed temperatures higher than 250°C to be released. No other gaseous nuclides were studied in this project.

The nuclides release through liquid leaching is conditioned by the porosity of the graphite and the water-repellent characteristic of it. The water do easily not penetrate and the porosity leads to decrease the penetration ratio due to the surface tension.

The leachant chemical characteristics play an important role (specially the pH) to reach a leaching rate enough high, it is necessary acidic pH and/or presence of chloride ions.

The kinetics of leaching was increased with the presence of complexants that produce the equilibrium between graphite surface and leachant displacement.

The leaching rate of i-graphite in deionised water is small and no constant in tendency.

7 REFERENCES

Basically the studies summarized comes from:

- Esteban Duque et al. TRATAMIENTO Y ACONDICIONAMIENTO DE GRAFITO RADIATIVO PROCEDENTE DE CENTRALES NUCLEARES. Final Report of CEC contract. N° FI.2D.0017.ES (JR). 1995
- G. Piña et al CHARACTERISATION OF RADIOACTIVE GRAPHITE FROM NPP DISMANTLING; Schriften- Forschungszentrum Julich Reihe Energietechnik; 27; 319-332. Proceedings on 4th International seminar, Radioactive waste products

[1] E. Gutierrez Rios "Química Inorgánica" Ed. Reverté, 1978

[2] M. Smiesek, S. Cerny, "Active Carbon", Elsevier Publishing Company, 1970

[3] A.G. Acheson U.S. Patent 1.030.372;1912

[4] J. Beck " Le goudron de hoille" PUF, 1966

[5] W.N. Reynolds ;Physical Properties of Graphite;Elsevier, 1968

[6] W.N. Reynolds; Chemistry and Pysics of Carbon", Vol2 Marcel Decker Inc, NY, 1968

[7] J.A.Suárez et al. (1997) Caracterización radiológica de grafito radiactivo. Proceedings of XXIII annual meeting of Sociedad Nuclear Española. 1997

[8] A Linares Solano PhD Thesis Granada University 1974

[9] S. Brunauer The adsorption of gases and Vapours Princeton University Press 1945

[10] T.L. Hill; Advances in Catalysis, Vol 4.; Academic Press 1958

[11] Washburn, E.W.; Proceedings of National Academy Science USA, 115, 7 1921

[12] A. G. de la Huebra; Estudio de camisas de grafito de la CN Vandellós I, Internal Report CIEMAT ITN/TR-OP-93;1993

[13] J. Rouquerol et al IUPAC Recommendations for the Characterization of Porous Solids; Pure & Appl. Chern., Vol. 66, No. 8, pp. 1739-1758, 1994.

[14] A. Esteban Duque, et al. Agua retenida en grafito Internal Report CIEMAT ITN/TR-88/II-94; 1994

[15] B. Fabrellas, A. Esteban Duque;Detección de Hidrogeno mediante desorción térmica y detección por IR; Internal Report CIEMAT DFN/TR-91/II-94; 1993.

[16] Raymond. A.. Devy. D. (1988). Determination du ⁵⁵Fe dans les effluents et dechets nucleaires. *Repport Technique RTDRDD N° 88205*. CEA. France.

- [17] Espartero. A.G.. Suárez. J.A.. Rodríguez. M. (1998). Determination of ^{93m}Nb and ^{94}Nb in medium and low level radioactive wastes. *Appl. Radiat. Isot.* **49**. 1277-1282.
- [18] A. Esteban-Duque et al. Treatment and conditioning of radioactive graphite from nuclear installations. Spectrum 92. International Topical Meeting on Nuclear and Hazardous Waste Management. 1992
- [19] A. G. de la Huebra et al. Caracterización de camisas de grafito irradiadas de la C.N. Vandellos I. CIEMAT Final Report ITN/TR-62/IF-94. 1994.
- [20] Estudio del contenido Isotópico del Grafito de la Central Nuclear de Vandellós 1; Internal Report CIEMAT ITN/TR-93/II-94; 1993
- [21] A. Esteban-Duque; Cinética de adsorción-desorción de sustancias hidrocarbonadas de Grafito; Internal Report CIEMAT ITN/TR-97/II-94; 1993.
- [22]] A. Esteban-Duque; Extracción de Volátiles del Grafito con Benceno Internal Report CIEMAT ITN/TR-99/II-94; 1993.
- [23] Gabriel Piña et al; Summary Report on Work Package 3; CW-D3000; 2012
- [24] Reporting Physisorption Data for Gas/Solid Systems with special reference to the Determination of Surface Area and Porosity; K. S. W. SING (IUPAC); Pure & Appl.Chem., Vol.54, No.11, pp.2201—2218, 1982. 0